Available online at www.sciencedirect.com
ScienceDirect
Journal of Contaminant Hydrology 93 (2007) 161–187
JOURNAL OF Contaminant Hydrology
www.elsevier.com/locate/jconhyd

Field-scale effective matrix diffusion coefficient for fractured rock: Results from literature survey ☆

Quanlin Zhou [a,*], Hui-Hai Liu [a], Fred J. Molz [b], Yingqi Zhang [a], Gudmundur S. Bodvarsson [a]

[a] *Earth Sciences Division, Lawrence Berkeley National Laboratory, University of California, Berkeley, CA 94720, United States*
[b] *Department of Environmental Engineering and Science, Clemson University, Clemson, SC 29634, United States*

Received 22 April 2006; received in revised form 13 January 2007; accepted 14 February 2007
Available online 22 February 2007

Abstract

Matrix diffusion is an important mechanism for solute transport in fractured rock. We recently conducted a literature survey on the effective matrix diffusion coefficient, D_m^e, a key parameter for describing matrix diffusion processes at the field scale. Forty field tracer tests at 15 fractured geologic sites were surveyed and selected for the study, based on data availability and quality. Field-scale D_m^e values were calculated, either directly using data reported in the literature, or by reanalyzing the corresponding field tracer tests. The reanalysis was conducted for the selected tracer tests using analytic or semi-analytic solutions for tracer transport in linear, radial, or interwell flow fields. Surveyed data show that the scale factor of the effective matrix diffusion coefficient (defined as the ratio of D_m^e to the lab-scale matrix diffusion coefficient, D_m, of the same tracer) is generally larger than one, indicating that the effective matrix diffusion coefficient in the field is comparatively larger than the matrix diffusion coefficient at the rock-core scale. This larger value can be attributed to the many mass-transfer processes at different scales in naturally heterogeneous, fractured rock systems.

Furthermore, we observed a moderate, on average trend toward systematic increase in the scale factor with observation scale. This trend suggests that the effective matrix diffusion coefficient is likely to be statistically scale-dependent. The scale-factor value ranges from 0.5 to 884 for observation scales from 5 to 2000 m. At a given scale, the scale factor varies by two orders of magnitude, reflecting the influence of differing degrees of fractured rock heterogeneity at different geologic sites. In addition, the surveyed data indicate that field-scale longitudinal dispersivity generally increases with observation scale, which is consistent with previous studies. The scale-dependent field-scale matrix diffusion coefficient (and dispersivity) may have significant implications for assessing long-term, large-scale radionuclide and contaminant transport events in fractured rock, both for nuclear waste disposal and contaminant remediation.

Keywords: Scale dependence; Matrix diffusion; Fractured rock; Tracer test; Solute transport; Heterogeneity

1. Introduction

The phenomenon of matrix diffusion in fractured rock has been the subject of considerable research interest over the past three decades, since Foster (1975) used it to interpret a groundwater tritium anomaly in field

☆ This paper is dedicated to our coauthor, Gudmundur S. Bodvarsson, who passed away unexpectedly on November 29, 2006. The coauthors at LBNL will greatly miss him, both as the leader of the Yucca Mountain Project (YMP) at LBNL and as a strong advocate for young scientists. Without his leadership in the YMP, we would not have the opportunity to do the research included in this paper.

* Corresponding author. Tel.: +1 510 486 5748.
E-mail address: QZhou@lbl.gov (Q. Zhou).

0169-7722/$ - see front matter © 2007 Elsevier B.V. All rights reserved.
doi:10.1016/j.jconhyd.2007.02.002

observations (e.g., Grisak and Pickens, 1980; Neretnieks, 1980). Direct laboratory and field evidence of matrix diffusion, defined originally as molecular diffusive mass transfer of a solute between flowing fluid within fractures and stagnant fluid in the rock matrix, has been obtained in terms of an observed solute penetration depth into a rock matrix (e.g., Birgersson and Neretnieks, 1990; Jardine et al., 1999; Polak et al., 2003). Indirect evidence has been obtained from multi-tracer tests, through the significant breakthrough curve separation of simultaneously injected tracers of different values of matrix diffusion coefficient (e.g., Garnier et al., 1985; Maloszewski et al., 1999; Karasaki et al., 2000; Reimus et al., 2003a,b). In a rock matrix, molecular diffusion would be the dominant transport process, with negligible fluid velocity and thus dispersion; within fractures, advection and dispersion are the two dominant transport processes (e.g., Tang et al., 1981; Sudicky and Frind, 1982; Maloszewski and Zuber, 1990, 1993; Moench, 1995). It is well documented in the literature that matrix diffusion is an important process for retarding solute transport in fractured rock, by allowing for solute storage within the often large void space of the matrix (e.g., Neretnieks, 1980; Zhou et al., 2003).

The matrix diffusion coefficient is a key parameter for describing the diffusion process in the rock matrix and the diffusive mass transfer between fractures and the matrix. Laboratory experiments on rock-matrix cores and field tracer tests at a larger scale have often been employed to estimate this coefficient (e.g., Skagius and Neretnieks, 1986; Ohlsson and Neretnieks, 1995; Ohlsson et al., 2001; Reimus et al., 2003b). It has been found that the lab-scale matrix diffusion coefficient may be orders of magnitude smaller than the field-scale value for the same geologic site, indicating that matrix diffusion in the field is enhanced in some way (e.g., Hodgkinson and Lever, 1983; Maloszewski and Zuber, 1993; Shapiro, 2001; Neretnieks, 2002; Liu et al., 2003, 2004a; Andersson et al., 2004). This enhancement may also be related to the significant inconsistency between rock properties (e.g., fracture aperture and matrix porosity) estimated from field tracer tests and those measured directly or estimated from hydraulic tests (e.g., Novakowski et al., 1985). The observed enhancement has been attributed to different mechanisms, including the existence of a degradation zone near the fracture–matrix interface (Hodgkinson and Lever, 1983; Zhou et al., 2006a), infilling materials and stagnant water within fractures (Johns and Roberts, 1991; Maloszewski and Zuber, 1993; Neretnieks, 2002), the effects of small-scale fractures (Wu et al., 2004), advective mass transfer between high- and low-permeability zones (Shapiro, 2001), and the potential fractal structure of transport paths in a fracture network (Liu et al., 2007). By compiling a few values of the field-scale, effective matrix diffusion coefficient at several geologic sites, Liu et al. (2004b) found that for fractured rock, the field-scale matrix diffusion coefficient might be scale-dependent. However, a comprehensive literature survey of the field-scale matrix diffusion coefficient in fractured rock is needed to further evaluate the potential scale-dependent behavior.

Many field tracer tests have been conducted in fractured rock since 1970 (e.g., Webster et al., 1970; Ivanovich and Smith, 1978; Garnier et al., 1985; Raven et al., 1988; Cacas et al., 1990b; Gustafsson and Andersson, 1991; Hadermann and Heer, 1996; Becker and Shapiro, 2000; Reimus et al., 2003a,b). A few long-term, large-scale transport events have also been observed in fractured rock systems (e.g., Bibby, 1981; Shapiro, 2001). These field tests and observations provide valuable data for investigating the field-scale matrix diffusion coefficient at different scales.

The objective of this study was to conduct a comprehensive literature survey of the field-scale matrix diffusion coefficient and to examine its potential scale-dependent behavior — mindful of the similar critical study of field-scale macrodispersivity scale dependence conducted by Gelhar et al. (1992). For studies with values of the effective matrix diffusion coefficient (D_m^e) reported directly or calculated indirectly from field tracer test analysis in the literature, the D_m^e values were directly cited. For those without such D_m^e values, reanalysis of the tracer tests was conducted to obtain the D_m^e values. The reported (or calculated) and reanalyzed D_m^e values are presented as a function of observation scale to examine the potential relationship between the effective matrix diffusion coefficient and observation scale.

With these goals in mind, we organize this paper as follows: First, we discuss the method used for obtaining the effective matrix diffusion coefficient in Section 2. Then, we present the values of the effective matrix diffusion coefficient determined from different field tests in Section 3. Finally, we provide interpretations of the data for the effective matrix diffusion coefficient (and dispersivity) in Section 4.

2. Determination of the field-scale matrix diffusion coefficient

2.1. Reanalysis of field tracer tests

For the field tracer tests without reported D_m^e values, reanalysis of the tracer breakthrough curves was needed

to calibrate transport parameters that included the effective matrix diffusion coefficient. This reanalysis was conducted using three existing solutions to tracer transport in different flow configurations: (1) the analytic solution for linear flow developed by Maloszewski and Zuber (1985, 1990), (2) the semi-analytic solution for radial flow by Reimus et al. (2003b), and (3) the numerical-analytic solution for interwell flow by Novakowski et al. (2004). These solutions and similar solutions (e.g., Tang et al., 1981; Sudicky and Frind, 1982; Novakowski, 1992) have been used for calibrating the D_m^e values reported in the literature. These analytic, semi-analytic and numerical-analytic solutions (henceforth referred to as analytic solutions) are given in Appendix A. For details of these solutions, the reader should refer to the original references.

Based on the analytic solutions in Appendix A, iTOUGH2-TRAT (Zhou, 2005) was developed using the inverse modeling package of iTOUGH2 for parameter estimation and sensitivity analysis (Finsterle, 1999). The iTOUGH2-TRAT code was used for reanalyzing selected field tracer tests. For each field test, we calibrated the following set of transport parameters:

$$T_0 = L/v, \tag{1}$$

$$P_e = vL/D = L/\alpha, \tag{2}$$

$$A = \frac{\phi_m}{b}\sqrt{R_m D_m}, \tag{3}$$

$$R_\phi = \frac{\phi_m}{\phi_f}(1-\phi_f), \tag{4}$$

where T_0 is the mean residence time of water, L is the distance between the tracer injection point and the observation point, v is the groundwater velocity in fractures, P_e is the Peclet number, D is the coefficient of hydrodynamic dispersion, α is the longitudinal dispersivity, A is the diffusive mass-transfer parameter, ϕ_m is the matrix porosity, D_m is the matrix diffusion coefficient, R_m is the retardation factor in the rock matrix (assuming a linear adsorption isotherm and instantaneous equilibrium), b is the half-fracture aperture, R_ϕ is the approximate ratio of matrix porosity to fracture porosity, ϕ_f (= b/B) is the fracture porosity, and B is the half-fracture spacing between neighboring parallel fractures. The diffusive mass-transfer parameter A (dim. $T^{-1/2}$) can be understood physically as square root of the inverse of the time needed for a fracture imbedded in a infinite rock matrix to reach a unit concentration in the matrix per unit concentration gradient (kept constant) at the fracture–matrix interface. Imagine a closed, stagnant fracture–matrix system of a unit fracture–matrix interface area, with solute flux from the matrix of initial unit concentration to the fracture initially solute-free. The governing equation for the mass transport is written as:

$$\frac{\partial c_f}{\partial t} = \frac{\phi_m D_m}{b}\frac{\partial c_m}{\partial z}, \tag{5}$$

where c_f ($0 \le c_f \le 1$) is the normalized fracture concentration, c_m ($\cong 1$) is the normalized matrix concentration, and z is the coordinate perpendicular to the fracture wall into the matrix. Assuming that the concentration gradient at the fracture–matrix interface is constant, the solution to Eq. (5) under the initial and boundary conditions is

$$A = \left(\frac{\phi_m}{bt_0}\Big/\frac{\partial c_m}{\partial z}\right)^{1/2}, \tag{6}$$

where t_0 is the time needed for the fracture to reach the equilibrium condition (with identical concentration for both the fracture and the matrix).

For a given set of transport parameters (T_0, P_e, A, and R_ϕ), the fracture concentration depends exclusively on the time since tracer injection, as observed in a withdrawal well. For the interwell tracer tests, the mean residence time (T_0) and Peclet number (P_e) calibrated and listed in this study correspond to the values of the shortest streamline between injection and withdrawal wells, as done in Maloszewski and Zuber (1993), because multiple streamlines are used in the numerical-analytic solution to represent complex flow fields caused by injection, pumping, and natural-gradient, and each streamline has different values of path length and travel time (see Appendix A).

2.2. Field-scale matrix diffusion coefficient

Note that the analytic solutions used in this study are valid only for a simplified fracture–matrix system with (1) parallel fractures of identical spacing, (2) constant fracture aperture, (3) constant fluid velocity (for linear flow), (4) constant dispersivity, and (5) constant matrix diffusion coefficient. In this case, T_0 (residence time) represents uniform advection, P_e represents the local-scale mechanical dispersion, and A represents the diffusive mass transfer between fractures and the rock matrix.

When the analytic solutions are used to calibrate a field tracer test, the calibrated transport parameters incorporate additional transport mechanisms not considered in the

idealized transport models described above, and thus are effective parameters. Under natural field conditions, the calibrated T_0 represents the mean residence time for different flow channels caused by aperture variability in single fractures and by different fractures in a fracture network. The calibrated P_e parameter represents the dispersion and spreading caused by the difference in velocity within and between different flow channels. The calibrated A parameter represents the complex mass-transfer processes between fractures and the rock matrix, as well as mass transport within rock mass. In this study, the calibrated parameters (T_0 and P_e) (and resulting dispersivity) were automatically referred to as effective parameters for field conditions. The effective, field-scale matrix diffusion coefficient ($D_{\mathrm{m}}^{\mathrm{e}}$) was used to differentiate it from the lab-scale matrix diffusion coefficient (D_{m}) measured at the lab-core scale. The $D_{\mathrm{m}}^{\mathrm{e}}$ value was calculated through the calibrated A value, mean fracture aperture, and mean matrix porosity, based on Eq. (3), as follows:

$$D_{\mathrm{m}}^{\mathrm{e}} = \frac{1}{R_{\mathrm{m}}}\left(\frac{Ab}{\phi_{\mathrm{m}}}\right)^2. \tag{7}$$

The effective matrix diffusion coefficient calibrated through a field tracer test represents various complex, site-specific mass-transfer processes, which are discussed in Section 4.1. Theoretically, these various mass-transfer processes can be simulated using the fundamental advection–diffusion equations, provided that various data on fractures (e.g., number of fractures, fracture connectivity, fracture aperture, fracture length) and the rock matrix (e.g., matrix porosity, diffusion coefficient, and their spatial variabilities) are available (Neretnieks and Moreno, 2003). In this case, the numerical model would be extremely complex, if not impossibly complex, and the spatially varying core-scale matrix diffusion coefficient can be directly used; no effective matrix diffusion coefficient is needed, because the lumped responses of the fractured rock system is simulated by tracking the advective and diffusive transport at the local scale. However, when dealing with large-scale, long-term transport events, it is impossible (and unnecessary) to collect all data needed to accurately represent the local-scale variabilities of the fractured rock system. As a result, large-scale transport is effectively simulated using a numerical model with large-sized gridblocks and spatially varying hydraulic and transport parameters, if needed. For each gridblock, the effective matrix diffusion coefficient is needed to represent the lumped transport features resulting from various small-scale mass-transfer processes within this gridblock. Fundamentally, field-scale matrix diffusion is an upscaled transport process based on local-scale matrix diffusion, which is similar to field-scale dispersion as an upscaled transport process from heterogeneous advection. It is believed that the field-scale, effective matrix diffusion coefficient homogeneous in a gridblock can produce the similar output as the local-scale matrix diffusion coefficient with consideration of spatially varying properties of fractures and the rock matrix within the gridblock.

Since the effective matrix diffusion coefficient calculated using Eq. (7) is related to the specific tracer used in field tests, we employed the scale factor (F_{D}) of the effective matrix diffusion coefficient to investigate its scale dependence. This scale factor was defined as the ratio of the effective matrix diffusion coefficient to the lab-scale matrix diffusion coefficient:

$$F_{\mathrm{D}} = \frac{D_{\mathrm{m}}^{\mathrm{e}}}{D_{\mathrm{m}}}. \tag{8}$$

Unlike the effective matrix diffusion coefficient, the scale factor was expected to be independent of individual tracers used in field tracer tests, but would depend on the scaling effects of fractured rock characteristics. The lab-scale matrix diffusion coefficient (D_{m}) used in Eq. (8) was the mean value of laboratory measurements for small rock-matrix samples from the same geologic site. When such measurements were not available, Archie's law (Boving and Grathwohl, 2001) was used to approximate this value, based on

$$D_{\mathrm{m}} = \phi_{\mathrm{m}}^{n-1} D_{\mathrm{w}}, \tag{9}$$

where D_{w} is the molecular diffusion coefficient of a tracer in free water, and n is an empirical parameter, which is generally larger than 2.0. To avoid potential exaggeration of scale effects (or an artificial increase in estimated F_{D} values), we used $n=2$ here. In the following sections, the effective matrix diffusion coefficient and its scale factor calculated for each tracer test are presented.

3. Field data on effective matrix diffusion coefficient

Field observations from some 40 fractured geologic sites (including results from field tracer tests conducted in different flow configurations and from naturally occurring isotopic tracer migration and contaminant transport events) were first collected from the literature. These observations were then used

for generating a data set of the effective matrix diffusion coefficients.

3.1. Field tracer tests and observations

Numerous field tracer tests were conducted in fractured rock in the 1970s and 1980s (e.g., Webster et al., 1970; Lenda and Zuber, 1970; Grove and Beetem, 1971; Kreft et al., 1974; Claassen and Cordes, 1975; Ivanovich and Smith, 1978; Gustafsson and Klockars, 1981; Tester et al., 1982; Black and Kipp, 1983; McCabe et al., 1983; Cullen et al., 1985; Garnier et al., 1985; Novakowski et al., 1985; Raven et al., 1988; Shapiro and Nicholas, 1989). These tests were conducted to estimate rock properties (e.g., fracture porosity and dispersivity) for groundwater flow and transport in fractured media for (1) nuclear waste disposal (e.g., Webster et al., 1970; Davison et al., 1982; Novakowski et al., 1985; Raven et al., 1988), (2) aquifer water resources (e.g., Black and Kipp, 1983), (3) geothermal reservoir production (e.g., Tester et al., 1982; Horne and Rodriguez, 1983; McCable et al., 1983), and others. The original analyses of these tests were based on advection–dispersion models, neglecting the effects of matrix diffusion (e.g., Zuber, 1974; Robinson and Tester, 1984; Shapiro and Nicholas, 1989). Some of these tests were reanalyzed and reported in the literature by using analytic models including matrix diffusion, which are the same as, or similar to, the analytic models in Appendix A (Hodgkinson and Lever, 1983; Maloszewski and Zuber, 1985; Bullivant and O'Sullivan, 1989; Maloszewski and Zuber, 1990, 1992, 1993; Moench, 1995). The reported values of the field-scale matrix diffusion coefficient were used directly as entries to our data set. Of the remaining tracer tests (without reported D_m^e values), some were selected based on data availability and quality (to be discussed in the following section) and reanalyzed to obtain the corresponding D_m^e values.

Since 1990, many field tests have been conducted, using conservative non-sorbing and reactive sorbing tracers, in natural-gradient flow (Himmelsbach et al., 1998; Jardine et al., 1999; Lapcevic et al., 1999; Maloszewski et al., 1999), induced linear flow (e.g., by infiltration) (Cacas et al., 1990b; Abelin et al., 1991a,b; Birgersson et al., 1993; McKay et al., 1993a; Sidle et al., 1998; Salve et al., 2004), induced convergent or weak-dipole flow (Jones et al., 1992; Cady et al., 1993; Hadermann and Heer, 1996; D'Alessandro et al., 1997; García Gutiérrez et al., 1997; Gylling et al., 1998; Himmelsbach et al., 1998; Hoehn et al., 1998; Becker and Shapiro, 2000; Karasaki et al., 2000; Meigs and Beauheim, 2001; Widestrand et al., 2001; Baumle, 2003; Lee et al., 2003; Reimus et al., 2003a,b; Andersson et al., 2004; Brouyère et al., 2004), induced divergent flow (Novakowski, 1992; Novakowski and Lapcevic, 1994), induced dipole recirculating flow (Frost et al., 1992; Scheier et al., 1993; Frost et al., 1995; Jakobsen et al., 1993; Sawada et al., 2000), induced single-well divergent–convergent flow (Meigs and Beauheim, 2001; Becker and Shapiro, 2003), and in more complicated flow (varying between tracer-source points to observation points) (Gustafsson and Andersson, 1991). Many of these tests were conducted using multiple tracers (e.g., Reimus et al., 2003a,b), multiple flow rates (e.g., Becker and Shapiro, 2000), and/or multiple flow configurations (e.g., Frost et al., 1995; Novakowski et al., 2004) to reduce the uncertainties (e.g., non-uniqueness) in calibrated transport parameters. In addition, in some of the tests, the bacteriophage and microsphere were injected simultaneously or separately with chemical tracers to separate the effects of matrix diffusion from advection and dispersion (Champ and Schroeter, 1988; Bales et al., 1989; McKay et al., 1993b; Becker et al., 1999; Reimus and Haga, 1999). At some geologic sites, tracer tests were conducted at different scales to investigate the scale effects of transport parameters (Novakowski and Lapcevic, 1994; Frost et al., 1995; Himmelsbach et al., 1998; Jardine et al., 1999; Maloszewski et al., 1999; Baumle, 2003). Most of these field tracer tests have been analyzed using analytic or numerical models considering matrix diffusion (e.g., Brettmann et al., 1993), and their reported values of field-scale matrix diffusion coefficients were again used as entries to our data set. Some of the remaining tracer tests without available coefficient (D_m^e) were reanalyzed to obtain the corresponding D_m^e values.

In addition to field tracer tests, a few isotopic tracer and contaminant transport events in regional groundwater flow within fractured rock have been observed (e.g., Bibby, 1981; Pankow et al., 1986; Johnson et al., 1989; Rudolph et al., 1991; Shapiro, 2001). The long-term, large-scale observations in some of these transport events (e.g., Bibby, 1981; Shapiro, 2001) are essential to our investigation of the field-scale matrix diffusion coefficient over a larger range of observation scales, because all field tracer tests were conducted at scales less than 1000 m.

3.2. Criteria for tracer test selection

Of the collected field observations from some 40 fractured geologic sites, only a fraction was selected to

Table 1
For selected fractured rock sites, a summary of the characteristics of geologic sites and tracer tests, spatial and time scales for observations, calibrated transport model parameters, effective matrix diffusion coefficients and the scale factor, and longitudinal dispersivity

1. Site name	2. References	3. Tracer tests
1. Poland, Poland	Lenda and Zuber, 1970; Maloszewski and Zuber, 1985	Well A–Well B (Test I–1)
	Kreft et al., 1974	Well A–Well B (Test I–3)
	Kreft et al., 1974; Maloszewski and Zuber, 1985	Well A–Well B (Test I–4)
	Zuber, 1974	Well B–Well C (Test II–4)
2. Chalk Aquifer, UK	Ivanovich and Smith, 1978; Maloszewski and Zuber, 1985	Borehole 5–Borehole 4
3. Finnsjon, Sweden	Hodgkinson and Lever, 1983; Zhou et al., 2006a	G2–G1
	Gustafsson and Andersson, 1991	KFI11–HFI01
4. Bethune, France	Garnier et al., 1985; Maloszewski and Zuber, 1990; Moench, 1995	Multi-tracer test
5. Chalk River, Canada	Novakowski et al., 1985	CR 6–CR 11
	Raven et al., 1988; Maloszewski and Zuber, 1993	Test 1 (FS6–FS15)
	Raven et al., 1988; Maloszewski and Zuber, 1993	Test 2 (FS15–FS6)
	Raven et al., 1988; Maloszewski and Zuber, 1993	Test 3 (FS6–FS15)
	Raven et al., 1988; Maloszewski and Zuber, 1993	Test 5 (FS6–FS11)
6. Red Gate Woods, IL	Shapiro and Nicholas, 1989; Maloszewski and Zuber, 1993	Test 070 (DH15–DH12)
7. Fany-Augeres, France	Cacas et al., 1990a,b; Maloszewski and Zuber, 1993	CH6–F3
	Cacas et al., 1990a,b; Maloszewski and Zuber, 1993	CH7-F2
8. Grimsel, Switzerland	Hadermann and Heer, 1996; Hoehn et al., 1998	GTS 4.9 m dipole test
9. Lindau, Germany	Himmelsbach et al., 1998	Flow 1
	Himmelsbach et al., 1998	Flow 2
	Himmelsbach et al., 1998	Flow 3
	Himmelsbach et al., 1998	Monopole V
	Himmelsbach et al., 1998	Monopole I
	Himmelsbach et al., 1998	Monopole VI
	Himmelsbach et al., 1998	Dipole I
	Himmelsbach et al., 1998	Dipole VI
	Himmelsbach et al., 1998	Monopole IV
	Himmelsbach et al., 1998	Dipole III
	Baumle, 2003	BL15–BL17
10. Lange Branks, Germany	Maloszewski et al., 1998	Test A (to HKLU)
	Maloszewski et al., 1998	Test A (HKLU to A3)
	Maloszewski et al., 1998	Test A (HKLU to HALB)
11. Oak Ridge, TN	Jardine et al., 1999	Wells 9 and 10
12. Mirror Lake, NH	Becker and Shapiro, 2000, 2003	FSE9–FSE6 (Test C)
	Shapiro, 2001	Environ. tracer observation
13. Aspo, Sweden	Neretnieks, 2002	STT1
	Andersson et al., 2004	C1/Path I
	Andersson et al., 2004	C3/Path III
14. Yucca Mountain, NV	Liu et al., 2003	Alcove 1
	Liu et al., 2004a	Alcove 8-Niche 3
15. Unknown, Canada	Novakowski et al. (2004)	S54A–S54D

examine the scale dependence of the effective matrix diffusion coefficient. Four major criteria were used for selecting the tracer tests used in this study.

First, the selected tracer tests had to be conducted in fractured rock that had a significant contrast between fracture and matrix permeability. Tracer tests conducted in other fractured porous media were not considered here. Examples of these fractured porous media are fractured tills immediately under the ground surface (McKay et al., 1993a,b; Sidle et al., 1998) and fractured permeable media with small permeability contrast (i.e., one or two orders of magnitude) and very small fracture length (Jones et al., 1992; Ostensen, 1998; Meigs and Beauheim, 2001). This criterion was based on the consideration that in fractured rock, diffusive mass transfer dominates the mass exchange at the fracture–matrix interface, and the estimated effective matrix diffusion coefficient is representative of the dominant diffusion process. However, in a fractured porous medium (with small permeability

4. Fractured material	5. Fractured zone thickness (m)	6. Matrix porosity	7. Fracture aperture (mm)	8. Conductivity (m/d) or transmissivity	9. Flow configuration
Zn–Pb deposits	46.2	0.064	0.59	40.6	Convergent
Zn–Pb deposits	46.2	0.064	0.47	40.6	Convergent
Zn–Pb deposits	48	0.064	0.40	50.0	Convergent
Limestone	7	0.064	0.20	9.7	Convergent
English chalk	13	0.15–0.4 (0.275)	0.11–0.19	0.70	Convergent
Granite	Single fracture	0.049	0.534	219.6	Convergent
	1 m	0.003	0.262	86.4	Natural-gradient
Chalk	15	0.39–0.43 (0.4)	0.25	4.0–5.3	Convergent
Monzonitic gneiss	Single fracture	0.003	0.06		Pure-dipole
	0.64		0.135		Pure-dipole
	0.64		0.135		Pure-dipole
	0.64		0.135		Convergent
	0.74		0.135		Pure-dipole
Silurian dolomite	Single fracture	0.02–0.18 (0.10)	2.90	0.02 m^2/s	Convergent
Granite	Flow paths	0.015	0.017–0.030	1.73e− 3	Induced linear flow (Infiltration)
					Induced linear flow (Infiltration)
Granite	0.05	0.15	0.093	3.80	Weak-dipole
Granite in a fault zone	0.3–3	0.041	0.434		Natural-gradient
			0.444		Natural-gradient
			0.576		Natural-gradient
			0.110	2.1–13	Natural-gradient
			0.237	0.5–2.1	Convergent
			0.256	0.5–2.1	Convergent
			0.107	0.5–2.1	Pure-dipole
			0.117	0.5–2.1	Pure-dipole
			0.237	0.7–35	Convergent
			0.268	0.7–35	Pure-dipole
			0.411		Convergent
Fault zone of fractured sandstone		0.023	0.232	1296	Natural-gradient
					Natural gradient
					Natural gradient
Shale bedrock	2.0	0.20	0.084	8.5	Natural-gradient
Crystalline bedrock	Single fracture	0.017	0.40	4.8 m^2/d	Weak-dipole
	Fracture zone	0.015			Natural-gradient
Crystalline rock	Single fracture	0.004	1.40		Convergent
	Fracture network		2.77		Weak-dipole
	Fracture network		15.0		Convergent
Welded tuff	Fracture zone	0.16			Infiltration in unsaturated zone
Welded tuff	Fault zone	0.11–0.15			Infiltration in unsaturated zone
Dolostone	Single fracture	0.08–0.10	0.649		Pure-dipole with regional flow

(continued on next page)

contrast), advective and dispersive mass transfer may exist between fractures and the matrix, and it is difficult to distinguish advective–dispersive mass transfer from diffusive mass transfer at the fracture–matrix interface. Also, solute transport in fractured media with very small fracture length (on the order of centimeters) may be similar to that in porous media, but is not typical for fractured rock, which is our focus here.

Second, the tracers used in the selected tests must be conservative. For non-conservative tracers, one or more additional parameters are needed to account for the corresponding adsorptive, reactive, or radioactive decay processes, complicating the transport–parameter calibration. In most cases, field tests of non-conservative tracers are conducted simultaneously with (or after) conservative tracer tests (e.g., Andersson et al., 2004). In practice, the conservative tracer tests are often used to determine the transport parameter set (T_0, P_e, A) for advection, dispersion, and matrix diffusion, and the non-conservative tracer tests are used to determine additional

Table 1 (*continued*)

10. Pumping rate (injection rate)	11. Tracer (injected mass)	12. Test scale L (m)	13. Test duration (h)	14. Fitted T_0	15. Fitted Pe	16. Fitted A ($s^{-1/2}$)
1730 L/min	Tritium (68.1 mCi)	22	65	2.5 h	3.0	2.37e−2
1400 L/min	Tritium (70.2 mCi)	22	65	5.0 h	4.5	2.23e−2
2000 L/min	Tritium (36.7e6 cpm)	21.3	40	5.7 h	22.1	6.07e−3
675 L/min	Tritium (27.2e6 cpm)	41.5	100	7.4 h	40.4	1.44e−2
3850 L/h	Tritium (20 mCi)	8	22	1.5 h	12.5	2.1e−2
72 L/h	Iodide	30	600	20.9 h	50.5	1.80e−3
3110 L/d	Uranine (12.89 g)	440	2688	50 d	19.3	3.57e−4
20,800 L/h	Deuterium (260 g)	10.2	23	0.64 h	50	40e−3
11.84 L/h (9.67 L/h)	Tritium (3.53 mCi)	10.6	30	6.3 h	10.6	1.68e−4
30 L/h	Tritium (27 MBq)	12.7	21	5.6 h	4.0	1.83e−3
32 L/h	Uranine (100 mg)	12.7	23	5.3 h	4.0	1.03e−3
14 L/h	Tritium (27 MBq)	12.7	60	34.5 h	4.3	1.0e−3
36.6 L/h	Tritium (40 MBq)	29.8	160	80.5 h	7.0	1.02e−3
3.96 L/s	Sodium chloride	19.8	2.5	27 min	31.3	6.5e−3
	Cr-EDTA	14	1800	190 h	12.5	1.42e−3
	Iodine NaI	16	720	11.2 h	7.7	7.5e−3
8.93 L/h (0.56 L/h)	Uranine	4.9	1000	19.6	19.6	19.6
1.5 L/s	Eosine (2.0 kg)	346	6000	432 h	100	2.36e−3
120 L/s	Uranine (2 kg)	235		160.8 h	60	3.80e−3
120 L/s	Pyranine (0.5 kg)	49		5.0 h	20	6.66e−3
0.127 L/s	Pyranine (10 g)	21.4		14.0 h	10	8.30e−3
0.098 L/s	Pyranine (2 g)	11.2	20	2.0 h	37	15.8e−3
0.096 L/s	Pyranine (2 g)	11.2		2.13 h	37	12.9e−3
0.126 L/s	Eosine (2 g)	11.2	10	0.7 h	67	15.5e−3
0.092 L/s	Uranine (2 g)	11.2		1.18 h	67	10.3e−3
0.127 L/s	Uranine (2 g)	16.2		1.30 h	18	11.4e−3
0.110 L/s	Pyranine (2 g)	16.2		0.78 h	66	6.96e−3
9.1 L/s	Bromide (388 g)	23	200	10 h	7.2	6.38e−3
	Bromide (multi-tracer)	11	1200	0.85 d	6.7	6.46e−3
	Bromide (multi-tracer)	225	1200	0.95 d	100	8.16e−3
	Bromide (multi-tracer)	330	7200	0.95 d	50	1.16e−2
	Bromide (multi-tracer)	6.0	480	1.44 h	60	0.178
174 L/h	Bromide (100 g)	36	400	27 h	15	3.36e−3
	Tritium and CFC-12	2000		23.5 y	8.0	
24 L/h	HTO (125 MBq)	4.7	600	6.0 h	5.0	
2.0 L/min (0.045)	Tritium (140 MBq)	16	200	14.6 h	8.5	1.35e−3
2.0 L/min	HTO (240 MBq)	33	3000	430 h	4.1	4.2e−4
	Bromide	30	8160			
	Bromide and PFBA	20	3840			
2.5 L/min	Bromide (334 mg), Lissamine (112 mg)	9.5	2.2			4.62e−3

parameters. In many tracer tests, multiple tracers of different values of the molecular diffusion coefficient are used to confirm the presence of matrix diffusion and to reduce the uncertainties involved in the calibration of transport parameters.

Third, a selected tracer test must be well defined, with clear breakthrough curves and detailed information on the tracer tests (e.g., injected mass, injection and pumping rates). These data are critical for accurate calibration of the transport parameters using the analytic models in Appendix A. A number of field tracer tests did not have detailed testing data documented in the literature (e.g., Claassen and Cordes, 1975; Cullen et al., 1985), and some other tracer tests were terminated too early, without the tailing limb recorded — for example, many tracer tests conducted in the 1970s to estimate fracture (advective) porosity and dispersivity recorded only the rising limb of breakthrough curves (e.g., Grove and Beetem, 1971). There were also some field tests in the literature conducted under natural-gradient flow

17. Method for reanalysis or reported	18. D_m^e (m^2/s)	19. D_m (m^2/s)	20. Scale factor F_D	21. Dispersivity α (m)	22. Velocity v (m/h)
Radial flow	1.19e−8	1.02e−10	116.1	7.4	8.73
Radial flow	6.53e−9		63.8	4.9	4.44
Radial flow	3.62e−10		3.5	0.96	3.77
Radial flow	4.96e−10		4.8	1.03	5.62
Reported	1.31e−10	1.0e−10	1.3	0.64	5.33
Reported	9.60e−11	6.10e−11	1.57	0.59	1.44
Linear flow	2.43e−10	1.35e−12	180	22.8	0.37
Reported	6.15e−10	1.0e−10	6.2	0.20	15.94
Interwell	2.82e−12	4.8e−12	0.59	1.00	1.68
Reported	6.78e−9	2.0e−10	33.9	3.20	2.27
Reported	2.15e−9	5.6e−11	38.4	3.20	2.40
Reported	2.03e−9	2.0e−10	10.2	2.95	0.37
Interwell	2.11e−9	2.0e−10	10.6	4.26	0.37
Reported	3.55e−8	1.5e−10	236.9	0.63	44.0
Reported	1.97e−11	6.75e−12	2.91	1.12	0.074
Reported	5.52e−10	3.0e−11	18.4	2.08	1.43
Reported	2.5e−11	5.5e−11	0.45	0.25	0.25
Reported	1.56e−10	1.85e−11	8.4	3.46	0.80
Reported	4.23e−10	1.85e−11	22.9	3.92	1.46
Reported	2.19e−9	6.15e−11	35.6	2.45	9.80
Reported	1.24e−10	6.15e−11	2.0	2.14	1.53
Reported	2.07e−9	6.15e−11	33.7	0.30	5.60
Reported	1.62e−9	6.15e−11	26.3	0.30	5.26
Reported	4.09e−10	1.85e−11	22.1	0.17	16.0
Reported	2.18e−10	1.85e−11	11.8	0.17	9.49
Reported	1.08e−9	1.85e−11	58.4	0.90	12.46
Reported	5.17e−10	6.15e−11	8.4	0.25	20.77
Radial Flow	1.02e−9	8.53e−11	12.0	3.19	2.30
Reported	1.06e−9	4.72e−11	22.5	1.64	0.54
Reported	1.69e−9		35.8	2.25	9.87
Reported	3.40e−9		72.0	6.60	14.47
Reported	1.39e−9	4.62e−10	3.0	0.1	4.17
Reported	1.62e−9	3.34e−11	48.5	2.4	1.33
Reported	3.20e−8	3.20e−12	884	250	0.010
Reported	1.54e−9	2.0e−11	77	0.94	0.78
Reported	8.75e−11	2.5e−11	3.5	1.88	1.10
Reported	2.25e−10	2.5e−11	9.0	8.05	0.077
Reported			18.0		
Reported			45.0		0.021
Reported	2.78e−10	4.05e−11	6.8	0.18	

conditions, and with too low a mass recovery (Tester et al., 1982; McCabe et al., 1983). Under these circumstances, it would be impossible to accurately estimate the field-scale matrix diffusion coefficient.

Finally, fracture aperture and matrix porosity must be available for calculating the effective matrix diffusion coefficient from the calibrated A parameter values. In many cases, the fracture aperture (independently determined from direct measurements, or from calculations using hydraulic or tracer tests) or matrix porosity (measured from matrix cores) was not available (e.g., Webster et al., 1970), because detailed site characterization had not been conducted for the given geologic sites.

3.3. Summary of observations

The literature sources and pertinent data characterizing each of the surveyed sites are summarized in Table 1. Blank entries in the table indicate that the information was not available from the literature. This

table summarizes information for purposes of comparison only. The details of a particular geologic site may be found in the original reference sources.

3.3.1. Fractured rock characteristics

As indicated by the fourth-through-eighth columns in Table 1 (from the left), the study sites represent a wide variety of fractured media and settings. Summarized in these columns is information on fractured materials, average thickness of the fracture zone or single fracture, mean matrix porosity, measured (or calculated) fracture aperture, and hydraulic conductivity or transmissivity. Fractured rock materials include granitic rock with small matrix porosity, fractured shale with medium matrix porosity, and fractured chalk with large matrix porosity. The effective thickness for a tracer test depends on whether the tracer tests are conducted within a single fracture or a fracture zone. In several tracer tests conducted in a single fracture, the thickness is the fracture aperture, ranging from 0.06 to 2.9 mm. For the other tests, tracer moves through a fracture zone with a number of fractures, and the thickness is the arithmetic average of the screen length of pumping and injection wells. In this case, the thickness ranges from 0.64 to 76 m. Matrix porosity is usually measured from intact rock-matrix cores. The matrix porosity in Table 1 ranges from 0.3% for granitic rock to 40% for chalk; for a given geologic site, the variability in matrix porosity may not be high. For example, the matrix porosity for the British Chalk ranges from 0.15 to 0.40, with the ratio (of maximum value to minimum value) less than 3. Fracture aperture is usually measured for a single fracture in the field, or calculated using the fracture porosity and fracture spacing measured from surveys of a fracture zone (Maloszewski and Zuber, 1993). Fracture aperture is also obtained from model calibration using hydraulic tests with drawdown or estimated roughly from fracture permeability and porosity (see Eq. (17) of Maloszewski and Zuber (1993)).

3.3.2. Tracer test characteristics

The ninth-through-thirteenth columns in Table 1 summarize the features of the tracer tests in determining transport parameters for each test. Summarized in these columns is information on flow configuration, injection and pumping flow rates, tracer type and tracer mass injected, observation scale (L), and tracer test duration. Flow configuration in Table 1 includes convergent, weak-dipole, pure-dipole, and natural-gradient flow. Controlled tracer tests may be conducted under ambient groundwater flow conditions (herein referred to as "natural-gradient tests") or under conditions in which the flow configuration is induced by pumping or injection. In a convergent flow field, the tracer is introduced in an injection well, and the corresponding breakthrough of tracer concentration is recorded in a distant pumping well. The injection flow rate for the tracer-mass injection period is negligible. In such a tracer test, a fraction of the injected tracer mass may stay within the injection borehole and not contribute to the breakthrough curve at the pumping well.

In a weak-dipole tracer test, both the injection well and pumping well are operating at different flow rates for the entire testing period. After the tracer-mass injection is complete, a small fraction (say 5%) of the pumped water (containing tracer) from the pumping well is re-injected into the injection well to flush the tracer mass remaining within the injection boreholes and to reduce the borehole storage effects. The pumping and injection flow rates remain unchanged through the entire tracer test. The pure-dipole tracer test is different from a weak-dipole test only in that in the former, the pumping and injection flow rates are identical, whether or not 100% of the pumped water is recirculated to the injection well. At some geologic sites, different tracer tests in different flow configurations have been conducted (Frost et al., 1995; Becker and Shapiro, 2000).

Different flow rates between the injection and pumping wells at the same site have been used in some tracer tests. In a multiflow-rate test (which is a set of tracer tests), the identical dispersivity and matrix diffusion coefficient is expected for different tests with varying flow rates, and the mean residence time varies with the flow rates. All the breakthrough curves obtained in the multiflow-rate test were used to reduce the uncertainties and non-uniqueness of the calibration.

The observation scale is the separation between the injection and pumping wells in induced flow configurations (e.g., convergent, weak-dipole, and pure-dipole flow fields), or the distance between the tracer-source point and the sampling location in a natural-gradient flow condition. The tracer test duration is the time length of a tracer test for concentration monitoring between the start and end of the tracer test. The observation scale and the tracer test duration (i.e., time scale) are used to derive the relationship between the scale factor of the field-scale, effective matrix diffusion coefficient and the spatial and time scales.

3.3.3. The set of fitted transport parameters

The fourteenth-through-seventeenth columns in Table 1 summarize the calibrated transport parameters: the mean residence time (T_0), the Peclet number (P_e), the mass-transfer parameter (A), and the method used for

reanalysis or reported. In most cases, the porosity ratio R_ϕ was insensitive to measured breakthrough curves (because the tracer mass penetration depth is small in comparison with the half-fracture spacing between neighboring fractures), and thus the single-fracture approximation (corresponding to the infinite fracture spacing) was used. For a tracer test with reported tracer test analysis in the literature (using the tracer transport models in Appendix A or similar models), we listed directly the reported transport parameter values. For the other tracer tests listed in Table 1, reanalysis was conducted to calibrate the transport parameter set against the measured tracer breakthrough curves and the method (or analytic solution) used is listed in the seventeenth column.

3.3.4. Matrix diffusion coefficients, scale factor, macrodispersivity, and mean groundwater velocity

The eighteenth-through-twenty-second columns in Table 1 summarize the effective matrix diffusion coefficient (D_m^e), the lab-scale matrix diffusion coefficient (D_m), the scale factor (F_D) of the effective matrix diffusion coefficient, the longitudinal macrodispersivity (α), and the mean groundwater velocity (v). The D_m^e value was calculated based on the reported (or reanalyzed) value of the mass-transfer A parameter, fracture aperture, and matrix porosity available in the literature. The lab-scale matrix diffusion coefficient is often obtained from laboratory "through-diffusion" experiments on rock-matrix cores for a given conservative tracer, and a mean lab-scale value can be calculated from measurements of different intact rock-matrix cores for a given site. The scale factor of the effective matrix diffusion coefficient ($F_D = D_m^e / D_m$) was calculated using the effective and lab-scale matrix diffusion coefficients, and was expected to be independent of the tracers used. The longitudinal macrodispersivity (α) is calculated from the calibrated Peclet number (P_e) and the observation scale, whereas the mean groundwater velocity is calculated from the calibrated mean residence time (T_0) and the observation scale.

4. Results and discussion

4.1. Enhancement of matrix diffusion at field scale

Table 1 lists 40 values of the effective matrix diffusion coefficient from 15 fractured geologic sites, obtained through the mass-transfer parameter A reported in the literature and reanalyzed in this study. The scale factor (F_D) of the effective matrix diffusion coefficient was calculated for each of these effective matrix diffusion coefficients. As shown in Table 1, the scale factor is generally larger than one, indicating that matrix diffusion at the field scale is enhanced compared to lab-core scale. To demonstrate whether such enhancement is independent of types of fractured rock, we separated the granitic rock, for which a large number of data points were available (possibly resulting from the intention to store nuclear waste in deep saturated granitic rock in many countries), from the others. The reason for isolating granite is that the lab-scale matrix diffusion coefficient and matrix porosity are usually small for that rock. As shown in Fig. 1, it seems that the scale factor of the field-scale matrix diffusion coefficient is not significantly different for granitic rock than for the other types of fractured rock. For granitic rock with small matrix porosity, the field-scale matrix diffusion coefficient is, on average, significantly larger than its corresponding lab-scale value, as indicated by the larger-than-one F_D value (with two exceptions). Although the lab-scale matrix diffusion coefficient is usually small for granite, the field-scale matrix diffusion coefficient is relatively large for most of the field tracer tests conducted in it. As a result, in analyzing a field tracer test conducted in a fractured granitic rock, matrix-diffusion enhancement cannot be neglected merely because of the common very small lab-scale value.

As demonstrated by many researchers in the literature, the observed enhancement of field-scale matrix diffusion may be attributed to complicated mass-transfer processes in a naturally heterogeneous fractured rock system. These complicated processes at different scales are exhibited in the calibrated mass-transfer parameter A and the effective matrix diffusion coefficient. At different sites, one or more mass-transfer processes may dominate, while others may not be as important. The cause of these complicated diffusive mass-transfer processes includes (1) presence of a degraded zone along fracture walls and infilling materials within fractures, (2) variability in fracture aperture within single fractures; (3) coexistence of differently scaled fractures (i.e., global-flow fractures, bypassed fractures, small fractures, and ultrasmall fractures) within a fracture network; (4) multirate diffusion processes caused by heterogeneity in the matrix porosity and diffusion coefficient within the rock matrix. Here we briefly list these mass-transfer processes to support the enhancement of field-scale matrix diffusion observed in this study.

First, the rock matrix may be highly heterogeneous (in porosity and diffusion coefficient) with the penetration depth into the matrix from fractures. An altered and degraded zone with relatively high matrix porosity may exist between fractures and the intact rock matrix (Zhou

et al., 2006a). The degraded zone may be a layer of fracture coating (Skagius and Neretnieks, 1986) or a layer of karstic rock (Maloszewski and Zuber, 1993). This zone may result from the variable degree of chemical alteration and recrystallization and a high frequency of micro-fractures stemming from deformation caused by tectonic forces (see Fig. 3 in Andersson et al., 2004). Its thickness and porosity varies in space, resulting in irregular matrix diffusion into the rock matrix (Novakowski et al., 2004). The higher matrix porosity in the degraded zone (than that in the intact rock matrix) may contribute to the enhancement of field-scale matrix diffusion (Hodgkinson and Lever, 1983; Maloszewski and Zuber, 1993; Andersson et al., 2004). In addition, infilling materials and fault gouge materials may be found within fractures. These materials are often unconsolidated materials consisting of altered wall rock fragments infilled with clays (Maloszewski and Zuber, 1993; Andersson et al., 2004). For a number of geologic sites listed in Table 1 (e.g., the Finnsjon, Sweden site and the Aspo, Sweden site), the degraded zone and infilling materials have been identified by surveying natural fractures and their surrounding rock (Skagius and Neretnieks, 1986; Andersson et al., 2004), and by different diffusion processes exhibited in observed breakthrough curves in field tracer tests (Zhou et al., 2006a).

Second, a natural fracture usually exhibits variability in its aperture (e.g., Brown and Scholz, 1985; Tsang et al., 1991; Novakowski and Lapcevic, 1994). Field- and laboratory-scale experiments and theoretical investigations strongly suggest that aperture variability may result in flow focusing and channeling in a single fracture plane (e.g., Tsang et al., 1988; Moreno et al., 1988). Based on the cubic law for fracture permeability, flow channels occur in the regions with large aperture, leaving the remaining regions with little or no global flow. The so-called large-aperture regions may occupy less than 20% of the entire fracture plane area, resulting in a smaller effective interface area for diffusive mass transfer between fractures and the matrix.

On the other hand, these large-aperture regions may be in contact with small-aperture regions, and diffusive mass transfer may occur between flowing water in the former (of a single fracture) and stagnant water in the latter (e.g., Johns and Roberts, 1991; Neretnieks, 2002). The solute mass diffused into the small-aperture regions from large-aperture regions may further diffuse into the rock matrix in contact with the small-aperture regions. For the case in which the aqueous diffusion coefficient is much larger than the matrix diffusion coefficient (e.g., in fractured granite), the diffusive mass transfer between flowing and stagnant water within fractures may be dominant in comparison with the mass transfer between flowing water in channels and stagnant water in the rock matrix (Johns and Roberts, 1991). As a result, the matrix diffusion coefficient is enhanced by the additional diffusive mass transfer within fractures (in comparison with fracture–matrix diffusion). The effective matrix diffusion coefficient calibrated using field tracer tests may represent this kind of enhancement. For example, this mechanism was used by Neretnieks (2002) to account for the value of the fitted matrix diffusion coefficient that was significantly larger than the lab-scale value for a tracer test conducted at the site of Aspo, Sweden, listed in Table 1.

Third, fractures exist at different scales. Within a fracture network, the global flow may carry solutes through only a fraction of connected fractures (backbones),

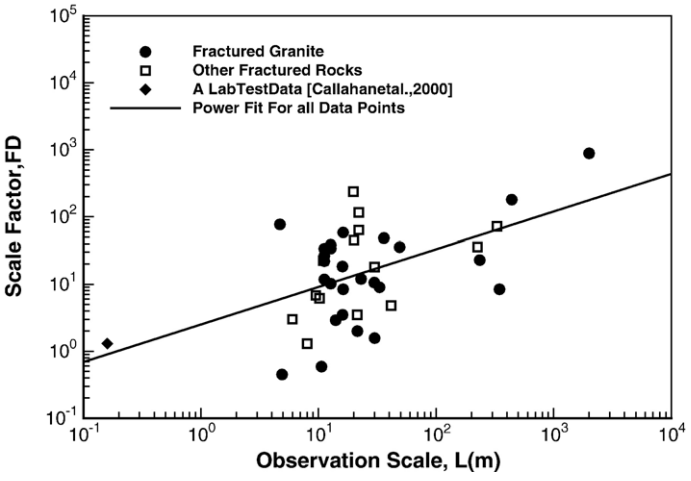

Fig. 1. Scale factor of the field-scale, effective matrix diffusion coefficient for different fractured rock sites as a function of observation scale.

leaving the remaining connected fractures bypassed by global flow (e.g., Rasmuson and Neretnieks, 1986). These bypassed fractures may, however, contribute to global transport by diffusive mass transfer between themselves and channels of global flow. In addition, there may be pervasive so-called small-scale fractures (Wu et al., 2004; Zhou et al., 2006b) usually neglected in field surveys, data processing (e.g., for fracture density and frequency), and modeling assessment. These small fractures may not contribute to global flow, but they do contribute to global transport by presenting additional paths for mass transfer between fractures and the matrix. This importance of small fractures to global transport has been supported by Wu et al. (2004), who developed a triple-continuum model consisting of the matrix, locally connected small-scale fractures, and globally connected large fractures. Therefore, field-scale matrix diffusion may also be enhanced by the mass transfer between global-flow fractures, bypassed fractures, small fractures, and ultra-small fractures.

Finally, the heterogeneity of intact rock-matrix properties may also play a role in enhancing the effective matrix diffusion coefficient. As a fracture network having different types of heterogeneity, the rock matrix has spatially varying matrix porosities and matrix diffusion coefficients from core scale to large scale. Within the core, the matrix diffusion coefficient may vary depending on heterogeneous porosity and formation factors, as evidenced by recent studies involving imaging techniques (e.g., Tidwell et al., 2000; Altman et al., 2004). The core-scale matrix diffusion coefficient is usually measured by through-diffusion experiments on a core of rock matrix under laboratory conditions (e.g., Callahan et al., 2000), and represents the lumped matrix diffusion coefficient for the core as a whole.

The core-to-core scale spatial variability in matrix porosity and diffusion coefficient has been demonstrated by sampling at different locations of a geologic site (Skagius and Neretnieks, 1986). Haggerty and Gorelick (1995) developed a multirate diffusion model to consider the pore-scale heterogeneity of diffusive properties. This model was successfully applied to fractured dolomite with small permeability contrast between fractures and the matrix (Fleming and Haggerty, 2001; Haggerty et al., 2001; McKenna et al., 2001).

Thus, the within-core and core-to-core variability in the matrix diffusion coefficient may introduce some uncertainty in the calculated scale-factor value. We believe that matrix-property heterogeneity may not be as important as the first three mechanisms (i.e., the degraded zone, aperture variability, and differently scaled fractures) in enhancing the field-scale matrix diffusion observed in this study, because penetration depth into the rock matrix is not substantial in any of the field tracer tests. However, this role of matrix-property heterogeneity in long-term, large-scale transport events may be much more important than observed here.

In summary, the number of complicated mass-transfer processes discussed above (among others) may result in the enhancement of field-scale matrix diffusion and the larger (than one) scale factor of the effective matrix diffusion coefficient. These processes may also contribute to the scale dependence observed in this study (to be discussed directly below).

4.2. Scale dependence of the effective matrix diffusion coefficient

In addition to enhanced matrix diffusion at field scale, Fig. 1 also shows the scale factor of the effective matrix diffusion coefficient as a function of observation scale. The general trend is for the scale factor to moderately increase with observation scale. The scale-factor value varies from 0.5 to 884 for the observation scale from 5 m to 2000 m. In addition, two clusters of data points for the scale factor and observation scale can be distinguished, because few data points are available in between the two scale clusters. Most field tracer tests are conducted at a small scale ($5 < L < 50$ m), and listed in the first cluster. In the second cluster, there are six data points for the scale over 100 m. The maximum observation scale for environmental tracers is on the order of 2000 m in a fractured crystalline rock (Shapiro, 2001), whereas the maximum scale for field tracer tests is 440 m in a fractured granitic rock zone (Gustafsson and Andersson, 1991). As can be seen, the observations at the over-hundred-meter scale are critical for the extrapolation of the effective matrix diffusion coefficient and the scale factor to a larger scale.

For a given scale, the scale-factor value varies over two orders of magnitude. This variance is particularly noticeable in the first cluster, because there are sufficient data points to characterize this variability; too few data points are available in the second cluster to define this variability for the observations at the over-hundred-meter scale. The variability in the scale-factor value for a given scale may be related to the heterogeneity of the fracture networks, the heterogeneity of the rock matrix, and the type of fractured rock (granite, chalk, or tuff).

The observed scale dependence of the field-scale, effective matrix diffusion coefficient may be attributed to the different mass-transfer mechanisms within a naturally heterogeneous fracture rock system, as discussed above for enhancing field-scale matrix

diffusion. However, it is difficult, if not impossible, to attribute the observed scale-dependence feature to a particular mechanism or a combination of mechanisms from field observation; the complicated fractured rock systems in the field are far from known, even for some geologic sites with extensive site characterization efforts, such as Yucca Mountain, Nevada (Bodvarsson and Tsang, 1999; Bodvarsson et al., 2003). The fact that geologic sites are complicated by spatially varying rock properties might be the reason for the repeated inability to demonstrate the scaling features of transport parameters through conducting field tracer tests with different scales at a particular site (Novakowski and Lapcevic, 1994; Frost et al., 1995; Himmelsbach et al., 1998; Jardine et al., 1999; Maloszewski et al., 1999; Baumle, 2003).

Alternatively, we conducted numerical experiments to demonstrate whether the scale dependence of the effective matrix diffusion coefficient exists, and under what conditions the scale-dependence feature occurs. Setup details for the numerical experiments and their findings were presented in our companion paper (Liu et al., 2007). Here, we briefly describe the findings to support our observations from field tracer tests. The experiments consisted of the following steps: (1) construction of a fracture network (using a deterministic recursive procedure), which included a singly connected major fracture (at Level 1) and a number of fractures of different levels looped to fractures of a lower level, to represent fractal scaling features of the fracture network; (2) calculation of flow rate through each fracture or loop and its corresponding velocity, assuming that fracture aperture is inversely proportional to the level of fractures,; (3) simulation of solute transport through the constructed fracture network, using the impulse–response function developed by Painter and Cvetkovic (2005), and particle tracking through the fracture network by accounting for the effects of varying fracture aperture on transport parameters; (4) calibration of the effective matrix diffusion coefficient against the breakthrough curves obtained at different locations (or length scales) along the major fracture, using the analytic solution of Tang et al. (1981) and the iTOUGH2-TRAT code (Zhou, 2005); (5) evaluation of the calibrated values of the effective matrix diffusion coefficient as a function of length scale and the combination of different features of the fracture network.

The findings of these numerical experiments can be summarized as follows

(1) The scale dependence of the effective matrix diffusion coefficient holds once there are fractures of different levels (or different scales) looped along a major flow path, as demonstrated by the increase in D_m^e values with length scale;
(2) Matrix diffusion into the surrounding rock matrix from fractures of multiple scales, including small-scale fractures, is the ultimate process for the enhancement and scale dependence of D_m^e, whereas advective transport from larger-scale (lower-level) fractures into small-scale (higher-level) fractures facilitates (in the small-scale fractures) the contribution of matrix diffusion to global transport. Otherwise, no scale dependence is observed, and transport occurs only within the major fracture and the surrounding rock matrix;
(3) The fractal scaling of the fracture network magnifies the scale dependence behavior of the effective matrix diffusion coefficient in comparison with the fracture network without the fractal scaling feature.

Note that the effective matrix diffusion coefficient defined with the numerical experiments is the parameter for mass transfer between the rock matrix and fractures, which was conceptualized as straight lines or planes, as in commonly used numerical and analytic models of solute transport. An actual fracture network is also generally conceptualized as parallel vertical or horizontal fractures, and a rough fracture wall is approximated as a flat wall. However, the actual solute–particle travel path is much more intricate and tortuous, because fracture network geometry can be characterized by fractals (e.g., Barton and Larsen, 1985; Molz et al., 2004). All contributions from matrix diffusion occurring between differently scaled fractures and their surrounding rock matrix can be attributed to the effective matrix diffusion coefficient, as in the averaging method used for any other upscaling (e.g., hydraulic conductivity in a heterogeneous porous media). In addition, the rough surface generates a much larger fracture–matrix interface area than a flat fracture wall, and that fracture roughness can be characterized by fractals (Wheatcraft and Tyler, 1988; Molz and Boman, 1993; National Research Council, 1996). The scale dependence of the field-scale matrix diffusion coefficient thus results from the upscaling of matrix diffusion occurring in fractures of various scales to the simplified transport model, which focuses on large-scale transport features and major flow paths.

In addition to the relationship between the scale factor of the field-scale, effective matrix diffusion coefficient and observation scale, we also observed the relationship between the scale factor and time scale of

tracer tests, and that between the scale factor and groundwater pore velocity. As shown in Fig. 2a, we do not observe the dependence of this scale factor on the tracer test duration, which ranges from 2.2 h to 340 days. This finding is consistent with that in numerical experiments conducted by Zhang et al. (2006). In these numerical experiments, the heterogeneity of the local-scale matrix diffusion coefficient with a lognormal distribution was considered using multirate diffusion processes, and the breakthrough curves at observation points were calculated using a modified particle-tracking method with analytic solution of tracer transport in single fractures. The advection residence time with a flow channel was varied by four orders of magnitude. The effective matrix diffusion coefficients were calibrated against the obtained breakthrough curve for each case of the tracer test duration. No apparent dependence of the effective matrix diffusion coefficient on the tracer test duration was observed.

However, our findings on the temporal-scale dependence of the field-scale matrix diffusion coefficient for fractured rock at the selected geologic sites are not consistent with those obtained by Haggerty et al. (2004) for porous and fractured media. Recently, Haggerty et al. (2004) indicated the temporal-scale dependence of mass-transfer coefficient for porous and fractured media, as a signature of the multirate diffusion processes, by compiling a larger number of tracer test results. They showed that the mass-transfer coefficient decreased with testing time for porous-medium results, but the trend was not obvious for fractured media (see their Fig. 1).

The mass-transfer coefficient used in Haggerty et al. (2004) was conceptually similar to the effective matrix

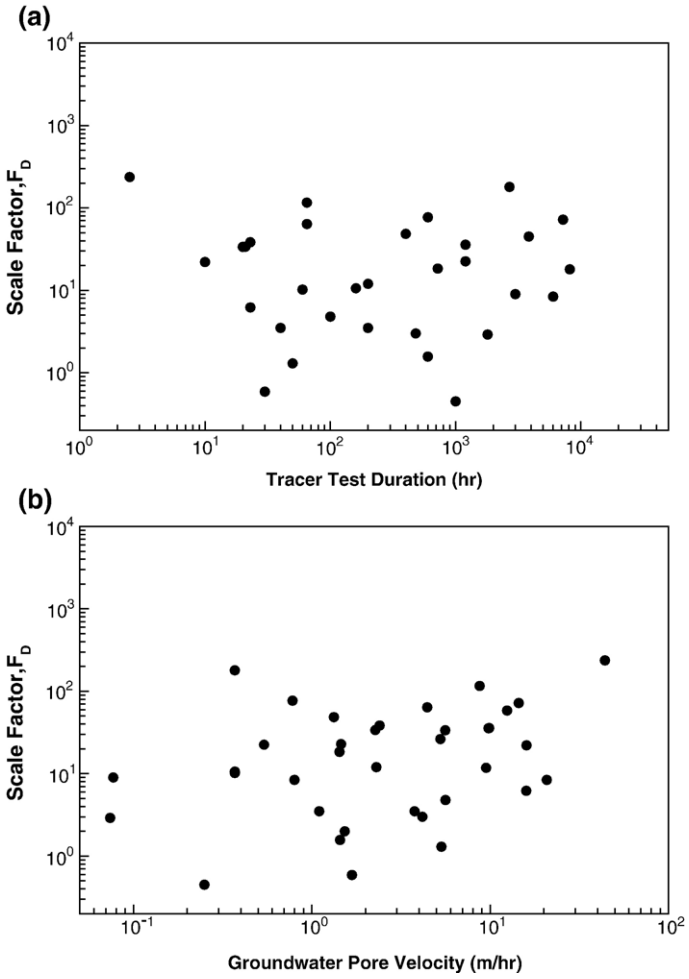

Fig. 2. Scale factor of the field-scale, effective matrix diffusion coefficient as a function of (a) the duration of tracer tests and (b) mean groundwater velocity.

diffusion coefficient here. The inconsistency between our findings and theirs may result from the fundamental differences between heterogeneous pore structures in porous media and complex fracture geometry (and its interaction with porous rock matrix) in fractured rock. One alternative explanation, however, is that most mass-transfer coefficients presented in Haggerty et al. (2004) were obtained using first-order mass-transfer models. These models generally overestimate the mass-transfer coefficient at early experiment periods, because of the existence of a sharp concentration gradient at the interface between mobile and immobile zones. In our analysis, however, the time-dependent concentration gradients at the fracture–matrix interface and the mass transfer from fractures to the matrix are captured analytically and exactly. As a result, overestimation is not an issue here.

As shown in Fig. 2b, we do not find a meaningful correlation between the scale factor of the effective matrix diffusion coefficient and pore velocity, which ranges from 0.01 to 44 m/h. This lack of correlation was also found by Haggerty et al. (2004) after analyzing a substantial number of tracer test results for fractured media. The common finding suggests that the advective mass-transfer mechanism in fractured rock may not be used to interpret for the enhancement of field-scale matrix diffusion and the scale dependence of the effective matrix diffusion coefficient. For a heterogeneous porous medium, however, the effective mass-transfer coefficient (conceptually similar to the effective matrix diffusion coefficient for fractured rock) increases with pore velocity, as demonstrated by Bajracharya and Barry (1997) and many others. More discussion of this correlation can be found in Bajracharya and Barry (1997) and Haggerty et al. (2004).

Our observation here is not consistent with the argument used by Shapiro (2001) in his interpretation of a kilometer-scale naturally occurring tracer transport event. To match tracer data observed at a kilometer scale, Shapiro (2001) needed a matrix diffusion coefficient that was orders of magnitude greater than that of laboratory experiments. (His analysis probably provides the first estimate for a kilometer-scale effective matrix diffusion coefficient in the literature.) He also suggested that the large, kilometer-scale effective matrix diffusion coefficient results from an advective process between high- and low-permeability zones, rather than from a real diffusive process. His argument was based mainly on studies of solute transport in heterogeneous porous media (Shapiro, 2001). However, as demonstrated in Fig. 2b, we do not see any correlation between pore velocity in fractures and the effective matrix diffusion coefficient for fractured rock sites. We believe that in fractured rock, diffusive transport dwarfs advective transport as a cause for mass transfer between fractures and the rock matrix, whereas the advective mass transfer between high- and low-permeability zones may be dominant in heterogeneous porous media. This is the reason that this study focused on field observations in fractured rock, excluding field tracer tests conducted in fractured porous media.

4.3. Scale dependence of field-scale dispersivity

In addition to the effective matrix diffusion coefficient, we also collected or estimated field-scale longitudinal dispersivity values for different tracer tests. The objective here is to evaluate the reasonableness of the calibrated values of the effective matrix diffusion coefficient in the context of calibrated longitudinal dispersivity values, as we check the consistency of the dispersivity data in this study against past studies of calibrated dispersivity versus scale.

As shown in Fig. 3, longitudinal dispersivity, in general, depends on observation scale. Field-scale dispersivity varies from 0.1 m to 250 m for a range of observation scales between 5 m and 2000 m. For the meters-scale tracer tests, this dispersivity is less than 1.0 m; for the tens-meter-scale tracer tests, this dispersivity is less than 10 m; for the hundreds-meter-scale tracer tests, this dispersivity is larger than 2.0 m but less than 23 m. The maximum dispersivity value of 250 m corresponds to the maximum scale of 2000 m (Shapiro, 2001), while the minimum dispersivity value of 0.1 is obtained for the multi-tracer test conducted in fractured shale bedrock (Jardine et al., 1999). For the tens-meter scale, sufficient data points of dispersivity are available to address its variability of one order of magnitude for a given scale. This variability may represent varying degrees of heterogeneity in fractured rock.

Shown in Fig. 4 is the comparison of our data set to that data set from Table 1 in Gelhar et al. (1992). They compiled dispersivity data to examine the scale-dependence behavior of field-scale macrodispersivity for both porous and fractured media. Their data were gathered from both field tracer tests and observations of environmental tracer migration in fractured and porous media, over a scale ranging from 0.75 to 100,000 m — whereas our data set corresponds to the field-scale dispersivity from controlled tracer tests (with one exception) in fractured rock over a smaller range of observation scales, between 5.0 and 2000 m.

It is also useful to compare our data set (for fractured rock) with the data set for fractured media only in Gelhar

et al. (1992). First, our data set can be classified as one of high quality, based on their selection criteria for high-quality data points. Only three of their data points for fractured media were included in our investigation, because their other data points did not meet our tracer test selection criteria. For example, the data point selected from Grove and Beetem (1971) in their data set was not considered in our study, because the recorded breakthrough curve contained the rising limb only — the falling limb was critical to accurately estimating dispersivity, by distinguishing the dispersion effect from the matrix diffusion effect.

Second, for the same tracer tests shared in both data sets, our calibrated dispersivity values are smaller than the corresponding values given in Gelhar et al. (1992) (see Fig. 4). Our dispersivity data were obtained by calibrating against the field tracer tests, using tracer transport models considering diffusive mass transfer between fractures and the matrix, as well as advection and dispersion in fractures. Their field-scale longitudinal dispersivity values were obtained by analyzing tracer tests using advection–dispersion models only, without consideration of matrix diffusion (Kreft et al., 1974; Ivanovich and Smith, 1978). When the advection–dispersion model is used to calibrate against a tracer test conducted in fractured rock with significant matrix diffusion effects, the Peclet number needs to decrease and the mean residence time needs to increase, to match the highly skewed breakthrough curve with long tailing (Maloszewski and Zuber, 1985, 1990, 1993; Moench, 1995; Reimus et al., 2003b). Still, in spite of the differences in the two data sets, the behavior of the scale-dependent macrodispersivity at the field scale revealed from the two data sets is similar. Macrodispersivity increases with observation scale for fractured rock shown in this study, at a slope close to that discovered by Gelhar et al. (1992) for both fractured rock and porous media.

The calibrated field-scale dispersion represents the mixing and spreading phenomena (1) across fracture apertures (i.e., one-dimensional mixing), (2) within fracture planes (i.e., two-dimensional mixing), and (3) within fracture networks (i.e., three-dimensional), as well as mixing at withdrawal wells by pumping water coming from different flow streamlines under dipole flow conditions (Novakowski et al., 2004). The one-dimensional across-aperture mixing in a constant-aperture fracture results from the non-uniform (parabolic) fluid velocity distribution across the fracture aperture, and from the molecular diffusion caused by the cross-aperture concentration gradient between fracture center of a high velocity and region adjacent to fracture walls of a lower velocity. The two-dimensional within-fracture mixing is caused by the spatial variability in fracture aperture, which leads to flow paths of varying flow rates (i.e., fast, preferential flow paths versus slow flow paths) (Detwiler et al., 2000). The three-dimensional within-network mixing is produced by the velocity difference between flow paths along connected fractures. The effects of the three types of mixing and spreading in the field cannot be easily distinguished from each other. However, the first two mixing and spreading processes can be seen in the calibrated dispersivity values from field tracer tests conducted in single-fracture systems.

In our data set, there are six tracer tests conducted in single fractures. The Peclet number varies from 5.0 to 160, and the dispersivity varies from 0.19 to 2.4 m. For a smooth fracture with constant aperture, the across-aperture mixing can be described by Taylor dispersion

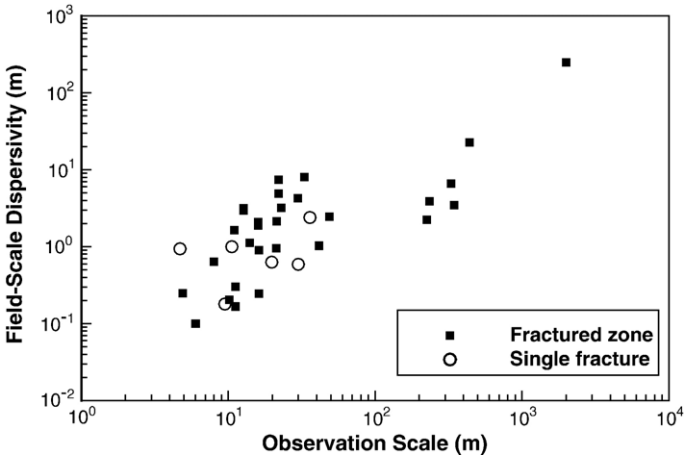

Fig. 3. Field-scale longitudinal dispersivities for fractured rock as a function of observation scale.

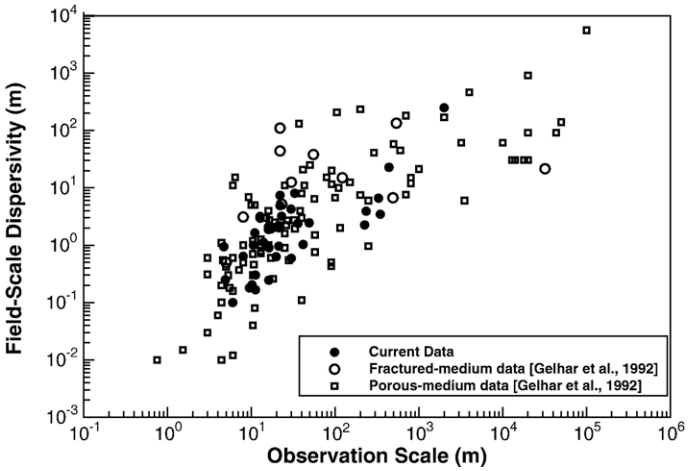

Fig. 4. Comparison of the scale dependence behavior of field-scale longitudinal dispersivities between this study (for fractured rock) and a previous study (for both porous and fractured media) (Gelhar et al., 1992).

(Taylor, 1953; Roux et al., 1998; Detwiler et al., 2000). The Taylor dispersion coefficient D_T, and dispersivity, α_T, can be written as:

$$D_T = \frac{1}{210}\frac{v^2(2b)^2}{D_w} \quad \text{and} \quad \alpha_T = \frac{1}{210}\frac{v(2b)^2}{D_w}. \qquad (10)$$

As shown in Eq. (10), the dispersivity of Taylor dispersion depends only on mean fluid velocity, fracture aperture, and the molecular diffusion coefficient in free water. It is independent of observation scale, because it describes the local cross-aperture mixing, rather than mixing within the fracture. We calculated the dispersivity values of Taylor dispersion (using the estimated mean velocity and fracture aperture) for the six tracer tests in single fractures and compared them with their calibrated field-scale dispersivity values. In all tests except one, the Taylor dispersivity is negligible (<1%) compared to the field-scale dispersivity. (The one exception is the tracer test of Shapiro and Nicholas (1989), in which both fracture aperture and velocity are very large, and the resulting Taylor dispersivity is 50% of the calibrated field-scale dispersivity.)

Therefore, the field-scale dispersivity (larger than Taylor dispersivity) must be caused by spatial variability in the velocity distribution within the fracture plane. This spatial variability may result from the variability of fracture aperture, as suggested by both *in situ* borehole observations and laboratory imaging of fracture samples (e.g., Novakowski and Lapcevic, 1994). Another reason for velocity variability may be the roughness of fracture walls. Consequently, the calibrated P_e parameter and resulting dispersivity is representative of the field-scale mixing phenomena caused by the heterogeneity in fracture aperture and roughness within a single-fracture system.

The third mixing and spreading process is evident in the calibrated dispersivity for the tracer tests conducted in fracture networks. For these tracer tests, the calibrated dispersivity is expected to represent the mixing between different fractures at their intersections or junctions (in addition to the first two mixing processes). The tracer mass through separated fractures may mix together at fracture intersections, leading to more spreading of tracer concentration caused by the heterogeneity between different fractures (Himmelsbach et al., 1998). The scale of such mixing depends on fracture connectivity and fracture length. In the case of small length, the mixing between different fractures may happen at small scale, whereas in the case of long fractures, mixing may happen only at the pumping well. In reality, many different-length fractures can intersect with each other, forming a well-connected fracture network. For a large-scale tracer test in a densely fractured rock zone, mixing between different fractures may happen at many different scales.

As a whole, we believe that field-scale longitudinal dispersivity was properly accounted for in the analyses of field tracer tests listed in Table 1, a belief supported by the consistency between our results and those in Gelhar et al. (1992). The obtained values of the field-scale matrix diffusion coefficient are thus shown to be reasonable.

4.4. Uncertainties

The calibration of the mass-transfer parameter A (for determining the effective matrix diffusion coefficient) and the Peclet number P_e (for determining the

field-scale longitudinal dispersivity) involves some degree of uncertainty and non-uniqueness — as with all other inverse modeling applications (e.g., Zhou et al., 2004). One major concern involved in the calibration is that both matrix diffusion and dispersion contribute to the mixing and spreading of tracer mass. For example, matrix diffusion usually produces long tailing in the observed breakthrough curves, but dispersion under a small P_e (e.g., $P_e<2$) condition also produces long tailing (e.g., see Fig. 2 in Maloszewski and Zuber, 1985). Given the resulting similarity, it is difficult to distinguish the effects of matrix diffusion from those of dispersion on the observed breakthrough curves.

However, more constraints (if available) can be used to reduce the calibration uncertainty. For all tracer tests reanalyzed in this study, we used various available data (e.g., measured fracture permeability, measured matrix porosity, and multiple flow rates and multiple tracers used in the tracer tests) to constrain the calibration. A very good example is the tracer test presented in Lenda and Zuber (1970), calibrated using the single-fracture advection–dispersion model with matrix diffusion by Maloszewski and Zuber (1985, Fig. 11). Their calibrated parameters were $T_0=28.8$ h, $P_e=0.33$, and $A=0.032$ $s^{-1/2}$, but the simulated breakthrough curve was not sensitive to the parameter values. In our reanalysis of this test, we also used another test (Kreft et al., 1974), conducted between the two wells at the same site with a reduced pumping flow rate (1.4 m^3/min), to constrain our calibration, thus obtaining a more reasonable parameter set: $T_0=2.5$ h, $P_e=3.0$, and $A=2.37\times10^{-2}$ $s^{-1/2}$ (see Table 1 and Fig. 5).

For some tracer tests with reported D_m^e values used in this study, calibrated D_m^e values were considered reasonable and reliable, because either the total number of transport parameters for calibration was reduced by available data, or multiple tracers and multiple flow configurations were used to constrain the transport parameter calibration (e.g., Novakowski et al., 2004). For example, in the field tracer test presented in Liu et al. (2004a), the mean residence time was measured by the travel time of the unsaturated flow front using electrical resistivity probes. The measured travel time was used to significantly improve their confidence in the calibration, because a large dispersivity value produces a much earlier tracer concentration peak than the mean residence time of water, whereas matrix diffusion produces a concentration peak at a later time than the mean residence time of water.

In addition to the uncertainties and non-uniqueness that factor into calibration of the mass-transfer parameter A, there are uncertainties in calculating the effective matrix diffusion coefficient through Eq. (7). These uncertainties stem from those in the estimates of matrix porosity and half-fracture aperture (b). Fracture aperture for a discrete fracture or a fractured zone is often estimated using hydraulic tests (e.g., Novakowski et al., 2004) separately conducted from field tracer tests or using the measurements of hydraulic heads during or before tracer tests (e.g., Himmelsbach et al., 1998). It is believed that the fracture apertures estimated from hydraulic tests represent the large fractures that are globally connected and flow conducting, whereas fractures with small apertures may not contribute significantly to the global flow, in the case of significant

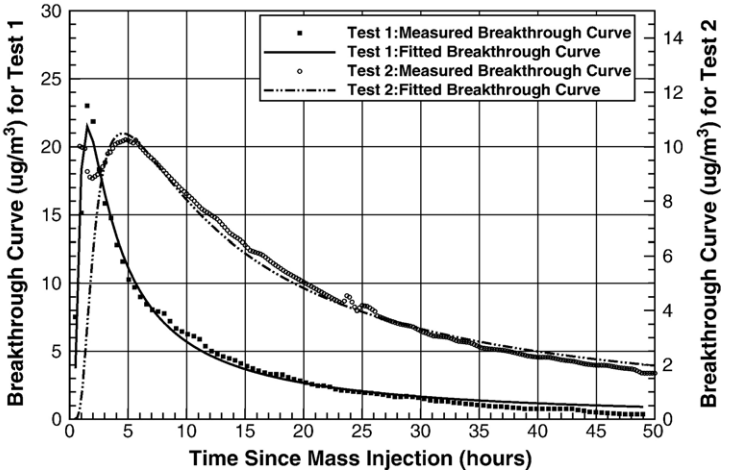

Fig. 5. Examples of fitting transport model parameters against measured breakthrough curves in two tracer tests conducted at the Poland site. (The measurement data are taken from Lenda and Zuber, 1970; Kreft et al., 1974; Maloszewski and Zuber, 1985).

heterogeneity in fracture apertures. Unlike global flow, global transport occurs within both large globally connected fractures and small-scale fractures, leading to a large range of fracture apertures contributing to global transport. However, using the hydraulic aperture estimated from field hydraulic tests in Eq. (7) is consistent with modeling practice, which focuses on large-scale features of flow and transport by ignoring the small-scale transport features.

There are also uncertainties in calculating the scale factor of the effective matrix diffusion coefficient. These uncertainties stem from the estimate of the lab-scale matrix diffusion coefficient (D_m). The lab-scale matrix diffusion coefficient used in Table 1 is the mean value of the core-scale matrix diffusion coefficient measured for a number of rock-matrix cores sampled from the same geologic site. This core-scale matrix diffusion coefficient is usually measured by through-diffusion experiments on a core of rock matrix under laboratory conditions (e.g., Callahan et al., 2000) and represents the lumped matrix diffusion coefficient for the core as a whole. The lab-scale matrix diffusion coefficient may also vary with different cores. Within-core and core-to-core variabilities may introduce uncertainties in the calculated scale-factor value. However, the mean lab-scale matrix diffusion coefficients used in this study are considered to be representative of the given geologic sites (e.g., Birgersson and Neretnieks, 1990; Fleming and Haggerty, 2001). When the core-scale value is unavailable, the mean matrix porosity was used to calculate the lab-scale matrix diffusion coefficient using Eq. (9). In this case, larger uncertainties in the calculated lab-scale matrix diffusion coefficient may occur.

5. Summary and conclusions

Matrix diffusion is an important process for retarding solute transport in fractured rock, and the matrix diffusion coefficient is a key parameter for describing this process. Previous studies have indicated that the values of the effective matrix diffusion coefficient obtained from field tracer tests are comparatively larger than their corresponding values of matrix diffusion coefficient at the laboratory core scale, and may increase with observation scale.

In this study, we conducted a comprehensive literature survey on the field-scale (effective) matrix diffusion coefficient D_m^e for fractured rock. Forty field tracer tests, including one field environmental tracer observation, at 15 geologic sites were selected for this survey, based on our data quality and availability criteria. For those with the calibrated mass-transfer parameter $A\left(=\frac{\phi_m}{b}\sqrt{D_m^e}\right)$ reported in the literature, the effective matrix diffusion values were calculated from the reported A values and available fracture aperture ($2b$) and matrix porosity (ϕ_m). For those tracer tests with unavailable A values, we reanalyzed these tracer tests using (semi- or numerical-) analytic solutions for tracer transport in linear, radial, and interwell flow fields. The D_m^e values calculated through the reanalyzed A values and the reported D_m^e values were used to develop the data set for investigating the potential scale dependence of the field-scale matrix diffusion coefficient. To focus exclusively on the scaling effects from the fractured rock characteristics, we calculated, for each D_m^e value, the scale factor (F_D) of the effective matrix diffusion coefficient, defined as the ratio of D_m^e to the lab-scale matrix diffusion coefficient (D_m).

Survey results indicate that the effective matrix diffusion coefficients in the field are comparatively larger than the matrix diffusion coefficients at the laboratory core scale, as indicated by the scale-factor values being generally larger than one. The results further show a possible trend toward systematic increase of the effective matrix diffusion coefficient with observation scale, indicating that the effective matrix diffusion coefficient, just like dispersivity and permeability (Neuman, 1990; Gelhar et al., 1992), is likely to be scale-dependent. The determined scale-factor values range from 0.5 to 884 for scales ranging from 5 to 2000 m. At a given scale, the scale-factor value varies by two orders of magnitude, reflecting the influence of differing degrees of fractured rock heterogeneity at different sites. Also, the survey results show that the field-scale longitudinal dispersivity appears to increase with observation scale, in a manner consistent with previous studies. The scale-dependent field-scale matrix diffusion coefficient (and dispersivity) may have significant implications for assessing long-term, large-scale radionuclide/contaminant transport events at fractured rock sites.

We believe that the additional, complex mass-transfer processes in a naturally heterogeneous fractured rock system may contribute to the enhancement of matrix diffusion at the field scale, as well as to the scale dependence of the field-scale matrix diffusion coefficient. A brief description of the mechanisms is given to support our field observations. However, it is difficult to define the effects of these mechanisms directly from field observations. Alternatively, using numerical experiments reducing the unknown complexity of a naturally fractured rock system, our research group focused on the particularly designed fractured rock system having a

large fracture surrounded by smaller fractures of multiple length scales. The experimental results demonstrated, for this fractured rock system, the dependence of the effective matrix diffusion coefficient on observation scale, with the smaller-scaled fractures diverting tracer mass from the large fracture to the fracture network, thus facilitating fracture–matrix mass transfer.

Acknowledgements

The authors wish to thank Allen Moench at the United States Geological Survey in Menlo Park, California, for providing his code for the numerical inversion of Laplace transform and his analytical solution for convergent flow systems. Thanks are also due to two anonymous reviewers for their constructive comments and suggestions, which helped to improve the quality of the manuscript, and to Guoping Lu and Daniel Hawkes at Lawrence Berkeley National Laboratory (LBNL) for their careful internal review. This report was prepared by LBNL pursuant to a contract funded by the United States Department of Energy (DOE), Office of Civilian Radioactive Waste Management (OCRWM), Office of Science and Technology and International (OST&I) and neither, LBNL nor any of its contractors or subcontractors nor the DOE/OCRWM/OST&I, nor any person acting on behalf of either: makes any warranty or representation, express or implied, with respect to the accuracy, completeness, or usefulness of the information contained in this report, or that the use of any information, apparatus, method, or process disclosed in this report may not infringe privately-owned rights; or assumes any liabilities with respect to the use of, or for damages resulting from the use of, any information, apparatus, method, or process disclosed in this report. Reference herein to any specific commercial product, process, or service by trade name, trademark, manufacturer, or otherwise, does not necessarily constitute or imply its endorsement, recommendation, or favoring by DOE/OCRWM/OST&I. The views, opinions, findings, and conclusions or recommendations of authors expressed herein do not necessarily state or reflect those of the DOE/OCRWM/OST&I.

Appendix A. Transport models for tracer test reanalysis

A.1. Tracer transport model in linear flow

The analytic solution of Maloszewski and Zuber (1985, 1990, 1993) was used for reanalysis of field tracer tests conducted in a linear flow configuration. The tracer transport equations for both fractures and the matrix under the linear flow condition can be written as follows:

$$\frac{\partial c_f}{\partial t}+\frac{v}{R_f}\frac{\partial c_f}{\partial x}-\frac{1}{R_f}\frac{\partial}{\partial x}\left(D\frac{\partial c_f}{\partial x}\right)-\frac{\phi_m D_m}{bR_f}\frac{\partial c_m}{\partial z}|_{z=b}=0, \tag{A.1}$$

$$\frac{\partial c_m}{\partial t}-\frac{D_m}{R_m}\frac{\partial^2 c_m}{\partial z^2}=0,\ \ b\le z\le B, \tag{A.2}$$

where subscripts f and m refer to fractures and the matrix, respectively, $c_f=c_f(x,t)$ and $c_m=c_m(x,z,t)$ are the tracer concentrations in fractures and the matrix, v is the groundwater velocity in fractures, R_f and R_m are the retardation factors, assuming a linear adsorption isotherm and instantaneous equilibrium, D is the hydrodynamic dispersion tensor, ϕ_m is the matrix porosity, D_m is the matrix diffusion coefficient, b is the half-fracture aperture, x is the Cartesian coordinate along the flow direction parallel to fractures, z is the coordinate perpendicular to the fracture plane, t is time, and B is the half-fracture spacing between neighboring parallel fractures.

The initial and boundary conditions for tracer transport in fractures and the matrix can be written as follows:

$$c_f(x,0)=c_m(x,z,0)=0, \tag{A.3.1}$$

$$c_f(\infty,t)=0, \tag{A.3.2}$$

$$c_m(x,b,t)=c_f(x,t), \tag{A.3.3}$$

$$\frac{\partial c_m(x,B,t)}{\partial x}=0, \tag{A.3.4}$$

$$c_f(0,t)=\frac{M}{Q}\delta(t) \tag{A.3.5}$$

where M is the total mass of a tracer (or activity of a radioactive tracer) injected, Q is the pumping rate at the withdrawal well or the flow rate with tracer mass, and $\delta(t)$ is the Dirac delta function. The corresponding analytic solution was given by Maloszewski and Zuber (1985):

$$c_f(t)=\frac{2M}{\pi^{3/2}Q}\exp\left(\frac{P_e}{2}\right)\int_w^\infty \exp\left[-\xi^2-\left(\frac{P_e}{4\xi}\right)^2\right]\times\int_0^\infty \eta\exp(-\varepsilon_1)\cos(\varepsilon_2)d\eta d\xi, \tag{A.4}$$

with

$$w = 0.5\left(\frac{P_e T_0}{t}\right)^{1/2}, \tag{A.5.1}$$

$$\varepsilon_1 = \frac{P_e T_0 A}{8}\frac{\eta}{\xi^2}\frac{\sinh(\varsigma)-\sin(\varsigma)}{\cosh(\varsigma)+\cos(\varsigma)}, \tag{A.5.2}$$

$$\varepsilon_2 = \frac{\eta^2}{2}\left(t-0.25P_e\frac{T_0}{\xi^2}\right)-\frac{P_e T_0 A}{8}\frac{\eta}{\xi^2}\frac{\sinh\ (\varsigma)+\sin(\varsigma)}{\cosh\ (\varsigma)+\cos\ (\varsigma)}, \tag{A.5.3}$$

$$\varsigma = \frac{R_m R_\phi}{A}\eta, \tag{A.5.4}$$

where ξ and η are two integration (dummy) variables. Note that the set of transport parameters (T_0, P_e, A, and R_ϕ) are defined in Eqs. (1)–(4).

When the solution is not sensitive to the R_ϕ parameter, the parallel-fracture model can be approximated by using the single-fracture model (Maloszewski and Zuber, 1990):

$$c_f(t) = \frac{MA}{4\pi Q}(P_e R_f T_0)^{1/2}\int_0^t \exp\left[-\frac{P_e(R_f T_0-\eta)^2}{4\eta R_f T_0}-\frac{A^2\eta^2}{4(t-\eta)}\right] \times \frac{d\eta}{(\eta(t-\eta)^3)^{1/2}}. \tag{A.6}$$

A.2. Tracer transport model in radial flow

The semi-analytic solution for a parallel-fracture system developed by Reimus et al. (2003b) was used for reanalyzing tracer tests conducted in a radial (or approximately radial) flow configuration. The transport equation for fractures in a radial flow system can be written as follows:

$$\frac{\partial c_f}{\partial t}+\frac{v(r)}{R_f}\frac{\partial c_f}{\partial r}-\frac{1}{R_f r}\frac{\partial}{\partial r}\left(rD\frac{\partial c_f}{\partial r}\right)-\frac{\phi_m D_m}{bR_f}\frac{\partial c_m}{\partial z}|_{z=b}=0, \tag{A.7}$$

where r is the radial coordinate along fractures and $v(r)$ is the groundwater pore velocity proportional to the distance from the withdrawal well.

The boundary condition, Eq. (A.3.5), can be changed to:

$$c_f(0,t) = \begin{cases} \dfrac{M}{Qt_p}, t \le t_p \\ 0, t > t_p \end{cases} \tag{A.8}$$

where t_p is the duration of mass injection. Note that other types of injection function can be derived using a very small t_p (for instantaneous injection) or a very large t_p (for constant-concentration injection).

By transforming and manipulating the transport equations, Eqs. (A.2) and (A.7), and the initial and boundary conditions, Eqs. (A.3.1)–(A.3.4) and (A.8), the analytic solution of the Laplace transform, $\bar{C}_f(s)$, of fracture concentration (Becker and Charbeneau, 2000; Reimus et al., 2003b), can be written as:

$$\bar{C}_f(s) = \frac{M}{Qt_p}\left(\frac{1-\exp(-t_p s)}{s}\right)\exp\left(\frac{P_e}{2}(1-r_{wL})\right) \times \frac{\mathrm{Ai}\left(\sigma^{1/3}\left(P_e+\frac{1}{4\sigma}\right)\right)}{\mathrm{Ai}\left(\sigma^{1/3}\left(r_{wL}P_e+\frac{1}{4\sigma}\right)\right)} \tag{A.9}$$

with

$$\sigma = \frac{2T_0}{P_e^2}\frac{s}{1-r_{wL}^2}\left[R_f+\frac{A}{\sqrt{s}}\mathrm{Tanh}\left(\frac{R_m R_\phi}{A}\sqrt{s}\right)\right], \tag{A.10}$$

where Ai() is the Airy function, r_{wL} (= r_w/r_L) is the ratio of the radius (r_w) of the pumping well to the separation (r_L) between injection and pumping wells, s is the Laplace variable. Note that the mean residence time is calculated using the mean groundwater velocity ($\bar{v}$) over the entire travel length.

The analytic solution in the Laplace domain, Eq. (A.9), can be inversely transformed numerically. We employed a numerical method developed by de Hoog et al. (1982) and extensively used for field tracer test analysis (e.g., Moench, 1991; Novakowski, 1992; Moench, 1995; Becker and Charbeneau, 2000). Through the numerical inversion of Eq. (A.9), the tracer concentration in fractures was calculated for a given transport parameter set (T_0, P_e, A, and R_ϕ) and other physical parameters. For short-term field tracer tests, tracer mass does not penetrate deeply into the rock matrix, so the observed tracer breakthrough curves are not sensitive to the fourth parameter R_ϕ. Consequently, only the first three parameters need to be calibrated for many tracer tests.

The semi-analytic solution was used for reanalyzing selected field tracer tests conducted in convergent and weak-dipole flow fields, which can be approximated as radial flow systems. In a weak-dipole flow field, a fraction (e.g., 5%) of pumped water (containing tracer mass) is reinjected into the injection well after the injection of the initial tracer-mass solution is complete. The effect of reinjection of tracer mass along with

pumped water can be accounted for as follows (Reimus et al., 2003b):

$$\bar{C}_{\mathrm{fR}}(s) = \frac{\bar{C}_{\mathrm{f}}(s)}{1-\omega\bar{C}_{\mathrm{f}}(s)}, \tag{A.11}$$

where $\bar{C}_{\mathrm{fR}}(s)$ is the analytic solution in the Laplace domain with tracer recirculation, $\bar{C}_{\mathrm{f}}(s)$ is the analytic solution without recirculation of tracer mass, and ω is the recirculation ratio ($0 \le \omega \le 1$).

A.3. Tracer transport model in interwell flow

For any interwell flow condition that cannot be approximated by linear or radial flow, we used a more general numerical-analytic method developed by Novakowski et al. (2004) for our reanalysis. In this method, the flow field is defined using streamlines constructed by superimposing the pumping regime, the injection regime, and the natural-gradient flow system. The one-dimensional tracer transport model, Eqs. (A.4) or (A.6), for linear flow was used to describe tracer transport along each streamline. The method is based on a particle-tracking routine in which the position of each particle at a given time $t+\Delta t$ is determined from:

$$x_i|_{t+\Delta t} = x_i|_t + \Delta t \sum_{j=1}^{2} \frac{Q_j}{2\pi\phi_{\mathrm{f}}B'} \frac{x_i|_t - X_j}{r_{ij}} + \Delta t V_x, \tag{A.12.1}$$

$$y_i|_{t+\Delta t} = y_i|_t + \Delta t \sum_{j=1}^{2} \frac{Q_j}{2\pi\phi_{\mathrm{f}}B'} \frac{y_i|_t - Y_j}{r_{ij}} + \Delta t V_y, \tag{A.12.2}$$

$$r_{ij} = [(x_i|_t - X_j)^2 + (y_i|_t - Y_j)^2]^{1/2}, \tag{A.12.3}$$

where y is the Cartesian coordinate perpendicular to the interwell direction along the fracture plane, Q_j is the volumetric pumping or injection rate of the jth well located at (X_j,Y_j), V_x and V_y are the regional groundwater velocity components in the x and y direction, respectively, B' is the thickness of a fracture zone, and Δt is the time-step size for particle tracking. For a single discrete fracture, the fracture aperture ($2b$) can be used to replace the term of $\phi_{\mathrm{f}}B'$ in Eqs. (A.12.1)–(A.12.3).

To determine the breakthrough curve at the withdrawal well, the tracer mass entering the flow domain at the injection well is apportioned according to the number of streamlines (particles) used in the flow solution. The concentration at the withdrawal well is determined by applying the solution in Eqs. (A.4) or (A.6) to the individual streamlines and combining the respective mass contributions. For each streamline, the streamline length and tracer travel time are calculated. When the time-step size (Δt) used for the particle tracking is very small, the method produces accurate simulation results for tracer transport in an interwell flow field, as demonstrated by Novakowski et al. (2004). Note that since each streamline has different values of path length and travel time, the mean residence time (T_0) and Peclet number (P_e) calibrated and listed in this study correspond to the values of the shortest streamline between injection and withdrawal wells, as done by Maloszewski and Zuber (1993).

References

Abelin, H., Birgersson, L., Gidlund, J., Neretnieks, I., 1991a. A large-scale flow and tracer experiment in granite, 1. Experimental design and flow distribution. Water Resour. Res. 27 (12), 3107–3117.

Abelin, H., Birgersson, L., Moreno, L., Widen, H., Agren, T., Neretnieks, I., 1991b. A large-scale flow and tracer experiment in granite, 2. Results and interpretation. Water Resour. Res. 27 (12), 3119–3135.

Andersson, P., Byegård, J., Tullborg, E., Doe, T., Hermanson, J., Winberg, A., 2004. In situ tracer tests to determine retention properties of a block scale fracture network in granitic rock at the Äspö Hard Rock Laboratory, Sweden. J. Contam. Hydrol. 70 (3–4), 271–297.

Altman, S.J., Uchida, M., Tidwell, V.C., Boney, C.M., Chambers, B.P., 2004. Use of X-ray absorption imaging to examine heterogeneous diffusion in fractured crystalline rocks. J. Contam. Hydrol. 69, 1–26.

Bajracharya, K., Barry, D.A., 1997. Nonequilibrium solute transport parameters and their physical significance: numerical and experimental results. J. Contam. Hydrol. 24, 185–240.

Bales, R.C., Gerba, C.P., Grondin, G.H., Jensen, S.L., 1989. Bacteriophage transport in sandy soil and fractured tuff. Appl. Environ. Microbiol. 55 (8), 2061–2067.

Barton, C.C., Larsen, E., 1985. Fractal geometry of two-dimensional fracture networks at Yucca Mountain, southwestern Nevada. Proc. Int. Symp. On Fundamentals of Rock Joints, Bjorkliden, Sweden, pp. 77–84.

Baumle, R., 2003. Geohydraulic characterization of fractured rock flow regimes, PhD thesis, Department of Applied Geology, University of Karlsruhe, Germany.

Becker, M.W., Charbeneau, R.J., 2000. First-passage-time transfer functions for groundwater tracer tests conducted in radially convergent flow. J. Contam. Hydrol. 40, 299–310.

Becker, M.W., Shapiro, A.M., 2000. Tracer transport in fractured crystalline rock: evidence of non-diffusive breakthrough tailing. Water Resour. Res. 36 (7), 1677–1686.

Becker, M.W., Reimus, P.W., Vilks, P., 1999. Transport and attenuation of carboxylate-modified-latex microspheres in fractured rock laboratory and field tracer tests. Ground Water 37 (3), 387–395.

Becker, M.W., Shapiro, A.M., 2003. Interpreting tracer breakthrough tailing from different forced-gradient tracer experiment configurations in fractured bedrock. Water Resour. Res. 39 (1), 1024. doi:10.1029/2001WR001190.

Bibby, R., 1981. Mass transport of solutes in dual-porosity media. Water Resour. Res. 17, 1075–1081.

Birgersson, L., Neretnieks, I., 1990. Diffusion in the matrix of granitic rock: field test in the Stripa mine. Water Resour. Res. 26 (11), 2833–2842.

Birgersson, L., Moreno, L., Neretnieks, I., Widén, H., Ågren, T., 1993. A tracer migration experiment in a small fracture zone in granite. Water Resour. Res. 29 (12), 3867–3878.

Black, J.H., Kipp Jr., K.L., 1983. Movement of tracers through dual-porosity media — experiments and modeling in the Cretaceous Chalk, England. J. Hydrol. 62, 287–312.

Bodvarsson, G.S., Tsang, Y. (Eds.), 1999. Yucca Mountain Project. J. Contam. Hydrol. vol. 38, pp. 1–146.

Bodvarsson, G.S., Ho, C.K., Robinson, B.A. (Eds.), 2003. Yucca Mountain Project. J. Contam. Hydrol. 62–63, p. 750.

Boving, T.B., Grathwohl, P., 2001. Tracer diffusion coefficients in sedimentary rocks: correlation to porosity and hydraulic conductivity. J. Contam. Hydrol. 53, 85–100.

Brettmann, K.L., Jensen, K.H., Jakobsen, R., 1993. Tracer test in fractured chalk, 2. Numerical analysis. Nordic Hydrol. 24, 275–296.

Brouyère, S., Dassargues, A., Hallet, V., 2004. Migration of contaminants through the unsaturated zone overlying the Hesbaye chalky aquifer in Belgium: a field investigation. J. Contam. Hydrol. 72 (1–4), 135–164.

Brown, S.R., Scholz, C.H., 1985. Closure of random elastic surfaces in contact. J. Geophys. Res. 90, 5531–5545.

Bullivant, D.P., O'Sullivan, M.J., 1989. Matching a field tracer test with some simple models. Water Resour. Res. 25, 1879–1891.

Cacas, M.C., Ledoux, E., de Marsily, G., Tillie, B., Barbreau, A., Durand, E., Feuga, B., Peaudecerf, P., 1990a. Modeling fracture flow with a stochastic discrete fracture network, calibration and validation, 1. The flow model. Water Resour. Res. 26, 479–489.

Cacas, M.C., Ledoux, E., de Marsily, G., Barbreau, A., Calmels, P., Gaillard, B., Margritta, R., 1990b. Modeling fracture flow with a stochastic discrete fracture network, calibration and validation, 2. The transport model. Water Resour. Res. 26, 491–500.

Cady, C., Silliman, S.E., Shaffern, E., 1993. Variation in aperture estimate ratios from hydraulic and tracer tests in a single fracture. Water Resour. Res. 29 (9), 2975–2982.

Callahan, T.J., Reimus, P.W., Bowman, R.S., Haga, M.J., 2000. Using multiple experimental methods to determine fracture/matrix interactions and dispersion of nonreactive solutes in saturated volcanic tuff. Water Resour. Res. 36 (12), 3547–3558.

Champ, D.R., Schroeter, J., 1988. Bacterial transport in fractured rock — a field-scale tracer test at the Chalk River Nuclear Laboratories. Water Sci. Technol. 20 (11/12), 81–87.

Claassen, H.C., Cordes, E.H., 1975. Two-well recirculating tracer test in fractured carbonate rock, Nevada. Hydrol. Sci. Bull. 20 (3), 367–382.

Cullen, J.J., Stetzenbach, K.J., Simpson, E.S., 1985. Field studies of solute transport in fractured crystalline rocks near Oracle, Arizona. IAH Memoirs vol. XVII,Part 1. Hydrogeology of Rocks of Low Permeability, Tucson, AZ, pp. 332–344.

D'Alessandro, M., Mousty, F., Bidoglio, G., Guimerte;, J., Benet, I., Sánchez-Vila, X., Gutiérrez, M.G., de Llano, A.Y., 1997. Field tracer experiment in a low permeability fractured medium: results from El Berrocal site. J. Contam. Hydrol. 26, 189–201.

Davison, C., Goblet, P., Neretnieks, I., 1982. Tracer Tests in Fissured Rock for Model Testing in INTRACOIN; Appendix 1, Introductory Description of Tracer Tests at Finnsjon and Summary of Important Data.

de Hoog, F.R., Knight, J.H., Stokes, A.N., 1982. An improved method for numerical inversion of Laplace transforms. SIAM J. Sci. Statist. Comput. 3 (3), 357–366.

Detwiler, R.L., Rajaram, H., Glass, R.J., 2000. Solute transport in variable-aperture fractures: an investigation of the relative importance of Taylor dispersion and macrodispersion. Water Resour. Res. 36 (7), 1611–1625.

Finsterle, S., 1999. ITOUGH2 User's Guide, Report LBNL-40040, UC-400. Lawrence Berkeley National Laboratory, Berkeley, CA.

Fleming, S.W., Haggerty, R., 2001. Modeling solute diffusion in the presence of pore-scale heterogeneity: method development and an application to the Culebra dolomite Member of the Rustler Formation, New Mexico, USA. J. Contam. Hydrol. 48, 253–276.

Foster, S.D., 1975. The chalk groundwater tritium anomaly — a possible explanation. J. Hydrol. 25, 159–165.

Frost, L.H., Scheier, N.W., Kozak, E.T., Davison, C.C., 1992. Solute transport properties of a major fracture zone in granite. In: Hotzland, W. (Ed.), Tracer Hydrology, pp. 313–320.

Frost, L.H., Scheier, N.W., Davison, C.C., 1995. Transport Properties in Highly Fractured Rock Experiment — Phase 2 Tracer Tests in Fracture Zone 2, At. Energy of Can. Ltd., Mississauga, Ontario. 65 pp.

García Gutiérrez, M.G., Guimerte;, J., Yllera de Llano, A., Hernández Benitez, A., Humm, J., Saltink, M., 1997. Tracer test at El Berrocal site. J. Contam. Hydrol. 26, 179–188.

Garnier, J.M., Crampon, N., Préaux, C., Porel, G., Vreulx, M., 1985. Traçage par 13C, 2H, I- et uranine dans la nappe de la craie sénonienne en écoulement radial convergent (Béthune, France). J. Hydrol. 78, 379–392.

Gelhar, L.W., Welty, C.W., Rehfeldt, K.R., 1992. A critical review of data on field-scale dispersion in aquifers. Water Resour. Res. 28 (7), 1955–1974.

Grisak, G.E., Pickens, J.F., 1980. Solute transport through fractured media, 1. The effect of matrix diffusion. Water Resour. Res. 16 (4), 719–730.

Grove, D.B., Beetem, W.A., 1971. Porosity and dispersion constant calculations for a fractured carbonate aquifer using the two-well tracer method. Water Resour. Res. 7 (1), 128–134.

Gustafsson, E., Klockars, C.E., 1981. Studies of Groundwater Transport in Fractured Crystalline Rock Under Controlled Conditions Using Nonradioactive Tracers, KBS 81-07.

Gustafsson, E., Andersson, P., 1991. Groundwater flow conditions in a low-angle fracture zone at Finnsjon, Sweden. J. Hydrol. 126, 79–111.

Gylling, B., Birgersson, L., Moreno, L., Neretnieks, I., 1998. Analysis of a long-term pumping and tracer test using the channel network model. J. Contam. Hydrol. 32, 203–222.

Hadermann, J., Heer, W., 1996. The Grimsel (Switzerland) migration experiment: integrating field experiments, laboratory investigations and modeling. J. Contam. Hydrol. 21, 87–100.

Haggerty, R., Gorelick, S.M., 1995. Multiple-rate mass transfer for modeling diffusion and surface reactions in media with pore-scale heterogeneity. Water Resour. Res. 31 (10), 2383–2400.

Haggerty, R., Fleming, S.W., Meigs, L.C., McKenna, S.A., 2001. Tracer tests in a fractured dolomite, 2. Analysis of mass transfer in single-well injection–withdrawal tests. Water Resour. Res. 37 (5), 1113–1128.

Haggerty, R., Harvey, C.F., Freiherr von Schwerin, C., Meigs, L.C., 2004. What controls the apparent timescale of solute mass transfer in aquifers and soils? A comparison of experimental results. Water Resour. Res. 40, W01510. doi:10.1029/2002WR001716.

Himmelsbach, T., Hotzl, H., Maloszewski, P., 1998. Solute transport processes in a highly permeable fault zone of Lindau fractured rock test site (Germany). Ground Water 36 (5), 792–799.

Hodgkinson, D.P., Lever, D.A., 1983. Interpretation of a field experiment on the transport of sorbed and non-sorbed tracers through a fracture in crystalline rock. Radioact. Waste Manag. Nucl. Fuel Cyle 4 (2), 129–158.

Hoehn, E., Eikenberg, J., Fierz, T., Drost, W., Reichlmayr, E., 1998. The Grimsel Migration Experiment: field injection–withdrawal

experiments in fractured rock with sorbing tracers. J. Contam. Hydrol. 34, 85–106.
Horne, R.N., Rodriguez, F., 1983. Dispersion in tracer flow in fractured geothermal systems. Geophys. Res. Lett. 10 (4), 289–292.
Ivanovich, M., Smith, D.B., 1978. Determination of aquifer parameters by a two-well pulsed method using radioactive tracers. J. Hydrol. 36, 35–35.
Jakobsen, R., Jensen, K.H., Brettmann, K.L., 1993. Tracer test in fractured chalk, 1. Experimental design and results. Nordic Hydrol. 24, 263–274.
Jardine, P.M., Sanford, W.E., Gwo, J.P., Reedy, O.C., Hicks, D.S., Riggs, J.S., Bailey, W.B., 1999. Quantifying diffusive mass transfer in fractured shale bedrock. Water Resour. Res. 35 (7), 2015–2030.
Johns, R.A., Roberts, P.V., 1991. A solute transport model for channelized flow in a fracture. Water Resour. Res. 27 (8), 1797–1808.
Johnson, R.L., Cherry, J.A., Pankow, J.F., 1989. Diffusive contaminant transport in natural clay: a field example and implications for clay-lined waste disposal sites. Environ. Sci. Technol. 23 (3), 340–349.
Jones, T.L., Kelley, V.A., Pickens, J.F., Upton, D.T., Beauheim, R.L., Davies, P.B., 1992. Integration of Interpretation Results of Tracer Tests Performed in the Culebra Dolomite at the Waste Isolation Pilot Plant, SAND92-1579, Sandia National Laboratories, Albuquerque, NM.
Karasaki, K., Freifeld, B., Cohen, A., Grossenbacher, K., Cook, P., Vasco, D., 2000. A multidisciplinary fractured rock characterization study at Raymond field site, Raymond, CA. J. Hydrol. 236 (1–2), 17–34.
Kreft, A., Lenda, A., Turek, B., Zuber, A., Czauderna, K., 1974. Determination of effective porosities by the two-well pulse method. Isotope Techniques in Groundwater Hydrology. Int. At. Energey Agency (I.A.E.A.), Vienna, pp. 295–312.
Lapcevic, P.A., Novakowski, K.S., Sudicky, E.A., 1999. The interpretation of a tracer experiment conducted in a single fracture under conditions of natural groundwater flow. Water Resour. Res. 35 (8), 2301–2312.
Lee, J.Y., Jim, J.W., Cheon, J.Y., Yi, M.J., Lee, K.K., 2003. Combined performance of pumping and tracer tests: A case study. Geosci. J. 7 (3), 237–241.
Lenda, A., Zuber, A., 1970. Tracer dispersion in groundwater experiments. Isotope Hydrology. Int. At. Energy Agency (I.A.E.A.), Vienna, pp. 619–641.
Liu, H.H., Haukwa, C.B., Ahlers, C.F., Bodvarsson, G.S., Flint, A.L., Guertal, W.B., 2003. Modeling flow and transport in unsaturated fractured rock: an evaluation of the continuum approach. J. Contam. Hydrol. 62–63, 173–188.
Liu, H.H., Salve, R., Wang, J.S., Bodvarsson, G.S., Hudson, D., 2004a. Field investigation into unsaturated flow and transport in a fault: model analyses. J. Contam. Hydrol. 74 (1–4), 39–59.
Liu, H.H., Bodvarsson, G.S., Zhang, G., 2004b. Scale dependency of the effective matrix diffusion coefficient. Vadose Zone J. 3, 312–315.
Liu, H.H., Zhang, Y., Zhou, Q., Molz, F.J., 2007. An interpretation of potential scale dependence of the effective matrix diffusion coefficient. J. Contam. Hydrol. 90, 41–57.
Maloszewski, P., Zuber, A., 1985. On the theory of tracer experiments in fissured rocks with a porous matrix. J. Hydrol. 79, 333–358.
Maloszewski, P., Zuber, A., 1990. Mathematical modeling of tracer behavior in short-term experiments in fissured rocks. Water Resour. Res. 26 (7), 1517–1528.
Maloszewski, P., Zuber, A., 1992. On the calibration and validation of mathematical models for the interpretation of tracer experiments in groundwater. Adv. Water Resour. 15, 47–62.
Maloszewski, P., Zuber, A., 1993. Tracer experiments in fractured rocks: matrix diffusion and the validity of models. Water Resour. Res. 29 (8), 2723–2735.
Maloszewski, P., Herrmann, A., Zuber, A., 1999. Interpretation of tracer tests performed in a fractured rock of the Lange Bramke Basin, Germany. Hydrogeol. J. 7, 209–218.
McCabe, W.J., Barry, B.J., Manning, M.R., 1983. Radioactive tracers in geothermal underground water flow studies. Geothermics 12 (2/3), 83–110.
McKay, L.D., Gillham, R.W., Cherry, J.A., 1993a. Field experiments in a fractured clay till, 2. Solute and colloid transport. Water Resour. Res. 29 (12), 3879–3890.
McKay, L.D., Cherry, J.A., Bales, R.C., Yahya, M.T., Gerba, C.P., 1993b. A field example of bacteriophage as tracers of fracture flow. Environ. Sci. Technol. 27, 1075–1079.
McKenna, S.A., Meigs, L.C., Haggerty, R., 2001. Tracer tests in a fractured dolomite, 3. Double-porosity, multiple-rate mass transfer processes in multiwell convergent-flow tracer tests. Water Resour. Res. 37 (5), 1143–1154.
Meigs, L.C., Beauheim, R.L., 2001. Tracer tests in a fractured dolomite, 1. Experimental design and observed tracer recoveries. Water Resour. Res. 37 (5), 1113–1128.
Moench, A.F., 1991. Convergent radial dispersion: a note on evaluation of the Laplace transform solution. Water Resour. Res. 27 (12), 3261–3264.
Moench, A.F., 1995. Convergent radial dispersion in a double-porosity aquifer with fracture skin: analytical solution and application to a field experiment in fractured chalk. Water Resour. Res. 31 (8), 1823–1835.
Molz, F.J., Boman, G.K., 1993. A stochastic interpolation scheme in subsurface hydrology. Water Resour. Res. 29, 3769–3774.
Molz, F.J., Rajaram, H., Lu, S., 2004. Stochastic fractal-based models of heterogeneity in subsurface hydrology: origins, applications, limitations, and future research questions. Rev. Geophys. 42, RG1002. doi:10.1029/2003RG000126.
Moreno, L., Tsang, Y.W., Tsang, C.F., Hale, F.V., Neretnieks, I., 1988. Flow and tracer transport in a single fracture: a stochastic model and its relation to some field observations. Water Resour. Res. 24 (12), 2033–2048.
National Research Council, 1996. Rock Fractures and Fluid Flow, Contemporary Understanding and Applications. National Academy Press, Washington, DC.
Neretnieks, I., 1980. Diffusion in the rock matrix: an important factor in radionuclide retardation? J. Geophys. Res. 85 (B8), 4379–4397.
Neretnieks, I., 2002. A stochastic multi-channel model for solute transport-analysis of tracer tests in fractured rock. J. Contam. Hydrol. 55, 175–211.
Neretnieks, I., Moreno, L., 2003. Prediction of some in situ tracer tests with sorbing tracers using independent data. J. Contam. Hydrol. 61, 351–360.
Neuman, S.P., 1990. Universal scaling of hydraulic conductivities and dispersivities in geologic media. Water Resour. Res. 26 (8), 1749–1758.
Novakowski, K.S., 1992. The analysis of tracer experiments conducted in divergent radial flow fields. Water Resour. Res. 28 (12), 3215–3225.
Novakowski, K.S., Lapcevic, P.A., 1994. Field measurement of radial solute transport in fractured rock. Water Resour. Res. 30 (1), 37–44.

Novakowski, K.S., Evans, G.V., Lever, D.A., Raven, K.G., 1985. A field example of measuring hydrodynamic dispersion in a single fracture. Water Resour. Res. 21 (8), 1165–1174.

Novakowski, K.S., Bickerton, G., Lapcevic, P., 2004. Interpretation of injection–withdrawal tracer experiments conducted between two wells in a large single fracture. J. Contam. Hydrol. 73, 227–247.

Ohlsson, Y., Neretnieks, I., 1995. Literature Survey of Matrix Diffusion Theory and of Experiments and Data Including Natural Analogues, Tech. Rep. 95–12. Swed. Nucl. Fuel and Waste Manag. Co. (SKB), Stockholm.

Ohlsson, Y., Lofgren, M., Neretnieks, I., 2001. Rock matrix diffusivity determinations by in-situ electrical conductivity measurements. J. Contam. Hydrol. 47, 117–125.

Ostensen, R.W., 1998. Tracer tests and contaminant transport rates in dual-porosity formations with application to the WIPP. J. Hydrol. 204 (1–4), 197–216.

Painter, S., Cvetkovic, V., 2005. Upscaling discrete fracture network simulations: an alternative to continuum transport models. Water Resour. Res. 41, W02002. doi:10.1029/2004WR003682.

Pankow, J.F., Johnson, R.L., Hewetson, J.P., Cherry, J.A., 1986. An evaluation of contaminant migration patterns at two waste disposal sites on fractured porous media in terms of the equivalent porous medium (EPM) model. J. Contam. Hydrol. 1, 65–76.

Polak, A., Grader, A.S., Wallach, R., Nativ, R., 2003. Chemical diffusion between a fracture and the surrounding matrix, measurement by computed tomography and modeling. Water Resour. Res. 39 (4), 1106. doi:10.1029/2001WR000813.

Rasmuson, A., Neretnieks, I., 1986. Radionuclide transport in fast channels in crystalline rock. Water Resour. Res. 22 (8), 1247–1256.

Raven, K.G., Novakowski, K.S., Lapcevic, P.A., 1988. Interpretation of field tracer tests of a single fracture using a transient solute storage model. Water Resour. Res. 24 (12), 2019–2032.

Reimus, P.W., Haga, M.J., 1999. Analysis of Tracer Responses in the BULLION Forced-gradient Experiment at Pahute Mesa, Nevada, LA-13615-MS. Los Alamos Natl. Lab, Los Alamos, NM.

Reimus, P.W., Haga, M.J., Adams, A.I., Callahan, T.J., Turin, H.J., Counce, D.A., 2003a. Testing and parameterizing a conceptual solute transport model in saturated fractured tuff using sorbing and nonsorbing tracers in cross-hole tracer tests. J. Contam. Hydrol. 62–63, 613–636.

Reimus, P., Pohll, G., Mihevc, T., Chapman, J., Haga, M., Lyles, B., Kosinski, S., Niswonger, R., Sanders, P., 2003b. Testing and parameterizing a conceptual model for solute transport in a fractured granite using multiple tracers in a forced-gradient test. Water Resour. Res. 39 (12), 1356. doi:10.1029/2002WR001597.

Robinson, B.A., Tester, J.W., 1984. Dispersed fluid flow in fractured reservoirs: an analysis of tracer-determined residence time distributions. J. Geophys. Res. 89 (B12), 10374–10384.

Roux, S., Plouraboue, F., Hulin, J.P., 1998. Tracer dispersion in rough open cracks. Transp. Porous Media 32, 97–116.

Rudolph, D.L., Cherry, J.A., Farvolden, P.N., 1991. Groundwater flow and solute transport in fractured lacustrine clay near Mexico City. Water Resour. Res. 27 (9), 2187–2201.

Salve, R., Liu, H.H., Cook, P., Czarnomski, A., Hu, Q., Hudson, D., 2004. Unsaturated flow and transport through a fault embedded in fractured welded tuff. Water Resour. Res. 40, W04210. doi:10.1029/2003WR002571.

Sawada, A., Uchida, M., Shimo, M., Yamamoto, H., Takahara, H., Doe, T.W., 2000. Non-sorbing tracer migration experiments in fractured rock at the Kamaishi Mine, Northeast Japan. Engineering Geology 56, 75–96.

Scheier, N.W., Frost, L.H., Davison, C.C., 1993. Groundwater tracer experiments in a major fracture zone in granite. In: Bank, S., Banks, D. (Eds.), AIH Memories XXIV Congress Hydrogeology of Hard Rocks, Part 2. Norway, Oslo, pp. 876–890.

Shapiro, A.M., 2001. Effective matrix diffusion in kilometer-scale transport in fractured crystalline rock. Water Resour. Res. 37 (3), 507–522.

Shapiro, A.M., Nicholas, J.R., 1989. Assessing the validity of the channel model of fracture aperture under field conditions. Water Resour. Res. 25 (5), 817–828.

Sidle, R.C., Nilsson, B., Hansen, M., Fredericia, J., 1998. Spatially varying hydraulic and solute transport characteristics of a fractured till determined by field tracer tests, Funen, Denmark. Water Resour. Res. 34 (10), 2515–2527.

Skagius, K., Neretnieks, I., 1986. Porosities and diffusivities of some nonsorbing species in crystalline rocks. Water Resour. Res. 22, 389–398.

Sudicky, E.A., Frind, E.O., 1982. Contaminant transport in fractured porous media: analytical solutions for a system of parallel fractures. Water Resour. Res. 18 (7), 1634–1642.

Tang, D.H., Frind, E.O., Sudicky, E.A., 1981. Contaminant transport in fractured porous media: analytical solution for a single fracture. Water Resour. Res. 17 (3), 555–564.

Taylor, G.I., 1953. Dispersion of soluble matter in solvent flowing slowly through a tube. Proc. R. Soc. Lond., A 219, 186–203.

Tester, J.N., Bivins, R.L., Potter, R.M., 1982. Inter-well tracer analysis of a hydraulically fractured granite geothermal reservoir. Soc. Pet. Eng. J. 22, 537.

Tidwell, V.C., Meigs, L.C., Christian-Frear, T.L., Boney, C.M., 2000. Effects of spatially heterogeneous porosity on matrix diffusion as investigated by X-ray absorption imaging. J. Contam. Hydrol. 42, 285–302.

Tsang, C.F., Tsang, Y.W., Hale, F.V., 1991. Tracer transport in fractures: analysis of field data based on a variable-aperture channel model. Water Resour. Res. 27 (12), 3095–3106.

Tsang, Y.W., Tsang, C.F., Neretnieks, I., Moreno, L., 1988. Flow and tracer transport in fractured media: a variable aperture channel model and its properties. Water Resour. Res. 24 (12), 2049–2060.

Webster, D.S., Procter, J.F., Marine, J.W., 1970. Two-well tracer test in fractured crystalline rock. U.S. Geol. Surv. Water-Supply Paper vol. 1544-I.

Wheatcraft, S.W., Tyler, S.W., 1988. An explanation of scale-dependent dispersivity in heterogeneous aquifers using concepts of fractal geometry. Water Resour. Res. 24, 566–578.

Widestrand, H., Byegård, J., Skarnemark, G., Skålberg, M., Andersson, P., Wass, E., 2001. In situ migration experiments at Äspö Hard Rock Laboratory, Sweden: results of radioactive tracer migration studies in a single fracture. J. Radioanal. Nucl. Chem. 250 (3), 501–517.

Wu, Y.S., Liu, H.H., Bodvarsson, G.S., 2004. A triple-continuum approach for modeling flow and transport processes in fractured rock. J. Contam. Hydrol. 73, 145–179.

Zhang, Y., Liu, H.H., Zhou, Q., Finsterle, S., 2006. Effects of diffusive property heterogeneity on effective matrix diffusion coefficient for fractured rock. Water Resour. Res. 42, W04405. doi:10.1029/2005WR004513.

Zhou, Q., 2005. Software Management Report for iTOUGH2-TRAT, Version 1.0, 1001-SMR-1.0-00. Lawrence Berkeley National Laboratory, Berkeley, CA.

Zhou, Q., Liu, H.H., Bodvarsson, G.S., Oldenburg, C.M., 2003. Flow and transport in unsaturated fractured rocks: effects of multiscale

heterogeneity of hydrogeologic properties. J. Contam. Hydrol. 60 (1–2), 1–30.

Zhou, Q., Birkholzer, J.T., Javandel, I., Jordan, P.D., 2004. Modeling three-dimensional groundwater flow and advective contaminant transport at a heterogeneous mountainous site in support of remediation. Vadose Zone J. 3, 884–900.

Zhou, Q., Liu, H.H., Bodvarsson, G.S., Molz, F.J., 2006a. Evidence of multi-process matrix diffusion in a single fracture from a field tracer test. Transp. Porous Media 63, 473–487. doi:10.1007/s11242-005-1123-9.

Zhou, Q., Salve, R., Liu, H.H., Wang, J.S., Hudson, D., 2006b. Analysis of a mesoscale infiltration and water seepage test in unsaturated fractured rock: spatial variabilities and discrete fracture patterns. J. Contam. Hydrol. 87, 96–122.

Zuber, A., 1974. Theoretical Possibilities of the Two-well Pulse Method, in Isotope Techniques in Groundwater Hydrology. Int. At. Energy Agency (IAEA), Vienna, pp. 277–294.